Journal of Molecular Liquids 338 (2021) 116658

Contents lists available at ScienceDirect

Journal of Molecular Liquids

journal homepage: www.elsevier.com/locate/molliq

Influence of critical parameters on nanoparticles-surfactant stabilized CO_2 foam stability at sub-critical and supercritical conditions

Nurudeen Yekeen [a,*], Tan Xin Kun [b], Ahmed Al-Yaseri [c], Farad Sagala [d], Ahmad Kamal Idris [b]

[a] Department of Chemical & Petroleum Engineering, Faculty of Engineering, Technology and Built Environment, UCSI University, No.1, Jalan Menara Gading, UCSI Heights (Taman Connaught), Cheras, 56000 Kuala Lumpur, Malaysia
[b] Department of Petroleum Engineering, School of Chemical and Energy Engineering, Universiti Teknologi Malaysia, 81310 Skudai, Johor Bahru, Malaysia
[c] Western Australia School of Mines, Minerals, Energy and Chemical Engineering, Curtin University, 26 Dick Perry Avenue, Kensington 6151, WA, Australia
[d] Department of Chemical and Petroleum Engineering, University of Calgary (UC), 2500 University Drive NW, Calgary, Alberta T2N 1N4, Canada

ARTICLE INFO

Article history:
Received 1 January 2021
Revised 30 May 2021
Accepted 2 June 2021
Available online 5 June 2021

Keywords:
CO_2 foam
Nanoparticles
Surfactant
Super-critical
Salinity
Oil

ABSTRACT

The stability of CO_2-foam stabilized via the synergy of nanoparticles and surfactants at downhole conditions is strongly affected by different process parameters such as temperature, CO_2 state, nanoparticles concentration, as well as resident brine and oil in the reservoir. Influence of critical parameters on static and dynamic stability of nanoparticles-surfactant stabilized CO_2-foam at sub-critical and super-critical conditions was investigated in this study. Firstly, extensive static and dynamic foam stability experiments were conducted at 80 °C and presence of 30 vol% hexadecane oil using formulation turbiscan, to screen different surfactants and nanoparticles. The best performing nanoparticles and surfactant were then selected at the screening stage for further foam stability tests to compare the performance of CO_2 foam at sub-critical and super-critical conditions. The foam stabilized by SiO_2 and sodium dodecyl sulfate (SDS) demonstrated consistent static and dynamic stability, with least spreading coefficient (-5.28 mN/m) and favourable Lamellae number (0.71). Increasing nanoparticles concentration increased the stability of sub-critical CO_2 foam whereas an optimum nanoparticles concentration for maximum stability of the supercritical CO_2 foam was obtained as 0.5 wt% SiO_2. The static stability of sub-critical and supercritical CO_2 foam increased with increased sodium chloride (NaCl) concentrations until 2 wt%. However, the super-critical CO_2 foam demonstrated increasing pressure drop and lowest reduction in mobility with increasing NaCl concentration until 10 wt%. Highly durable foams were generated when oil with high viscosity, high density and high molecular weight oil was added into the foaming dispersions. Mechanistic investigation of foam stabilization revealed that thickness of pseudo-emulsion films, as well as particles adsorption and orientation at gas–liquid and liquid–liquid interface, are key controlling parameters of foam static and dynamic stability in presence of oil, brine and at high temperature.

1. Introduction

Nearly 60% of original oil in place is trapped in reservoir after primary and secondary recovery processes due to undesirable rock and fluid properties, as well as reservoir heterogeneity [1]. Enhanced oil recovery (EOR) methods like thermal injection, chemical injection, and gas injection are used for the recovery of the remaining oil in the reservoir. Gas injection remains one of the most versatile and commonly utilised technologies with contribution of almost 40% to the worldwide hydrocarbon recovery [2]. The injection of CO_2 gas into hydrocarbon reservoir provides an innovative solution for mobilization of trapped hydrocarbon, as well as reduction of anthropogenic greenhouse gases emission. The high miscibility of CO_2 with the resident oil at the minimum miscibility pressure promotes hydrocarbon recovery through oil-viscosity and oil–water interfacial tension reduction. Thus, the oil hitherto trapped by capillary forces become a mobile phase.

But, CO_2 gas has higher mobility, lower density and its viscosity is lower than that of reservoir resident brine and oil, leading to gravity override and viscous fingering during CO_2 gas injection. Reservoir heterogeneity causes the injected fluid to flow into the higher permeability layer, bypassing the trapped oil at low permeable zone. CO_2 foamed injection has been proposed as a method of CO_2 gas mobility reduction. Laboratory experimental results showed that injected fluids can be successfully diverted to recover the trapped hydrocarbon in low permeable region of heterogenous reservoirs by foam, suggesting that gravity segregation, viscous

* Corresponding author.
E-mail address: peteryekeen@yahoo.com (N. Yekeen).

https://doi.org/10.1016/j.molliq.2021.116658
0167-7322/

fingering, and premature gas breakthrough usually associated with CO_2 gas flooding EOR, could be abated through CO_2 foam injection [3,4].

Surface-active agents are required for successful foam generation and stability. Feasibility of durable foam generation using polymers, surfactants and ionic liquids have been demonstrated in previous studies [5–15]. Results showed that the thermodynamically unstable foam could become kinetically stable due to the aggregation of the adsorbed molecules at thin-liquid films [2]. But the field application of the conventional foams has not been very successful. The thin liquid films become highly unstable at elevated temperature, pressure and extreme brine salinities. Foams that were stable for hours in the laboratory conditions could collapse within seconds on interaction with resident oil and brines at downhole conditions. Coupled with these challenges, are formation damage from the higher molecular weight polymers of polymer-enhanced foam, as well as the significant loss of surfactants molecules due to their retentions in porous formation, associated with surfactant-stabilized foam [16,17].

Due to the limitations of the conventional foams, significant attentions have been focused within the last two decades on foam stabilization through the synergy of nanoparticles and surfactant [5,18]. Nanoparticles were found to be irreversibly adsorbed at the foam lamellae because of their superior adhesion interfacial energy [19], resulting in generation of durable foams with high initial foamability and long-time stability. Significant reduction in water–oil interfacial tension by nanoparticles-surfactant complex reduces the capillary pressure for stable lamellae generation at pore throats. It is hypothesized that foam stabilization via the synergy of nanoparticles and surfactants could result in breakthrough in prospective field applications of foam for EOR purposes.

Bayat et al. [20] examined the impact of silicon dioxide (SiO_2), copper oxide (CuO), aluminium oxide (Al_2O_3), and titanium dioxide (TiO_2) nanoparticles on CO_2-foam stability. The nanoparticles concentration required for achieving the most durable static foam was identified as 0.008 wt% while the highest oil recovery (71.7%) from quartz sand porous media was achieved by nanosilica-stabilized CO_2-foam. However, the bulk screening stability experiments for the different types of nanoparticles were conducted in absence of oil, and at low temperature not representative of reservoir conditions. Emrani and Nasr-El-Din [21] found that Fe_2O_3 and SiO_2 nanoparticles presence in guar-gum and alpha olefin sulfonate solutions significantly improved the CO_2 foam stability. But, the stability of the CO_2 foam at sub-critical and supercritical conditions was not compared in their studies.

Srivastava et al. [22] examined the impact of polymers and nanosilica on the durability of sodium dodecylbenzene sulfonate (SDBS)-generated foam in aqueous media, consisting of 50% each of liquid paraffin and water. Results of their experiments indicated that the adsorption of the foam stabilizing agent at gas/liquid and liquid–liquid interface is essential for ensuring foam stability in oil presence. Pal et al. [23] demonstrated that durable viscoelastic foam, with pseudoplastic flow properties can be produced via the synergy of Gemini surfactant and nanoparticles (nanosilica and boron nitride nanoparticles). Srivastava et al. [22] and Pal et al. [23] experiments were limited to static stability and foam rheology. Foam stability at dynamic conditions were not extensively investigated.

Kang et al. [24] recently conducted microscopic and sand packed experiments. They reported that the synergy of SiO_2 nanoparticles and surfactant (nonionic-anionic mixtures) can produce durable foam at 85℃ in presence of 60,000 mg/L formation water, that can control the mobility of CO_2 foam in Changqing Oilfield. Ahmed et al. [25] also recently examined supercritical CO_2 foam rheological properties at varying temperature, foam qualities and pressure. Yang et al. [19] studied the application of synergy of nanoparticles and lauryl alcohol polyoxyethylene ether ($C_{12}E_{23}$) for CO_2 foam stabilization via static stability experiments, pore-scale visualization in micromodels and sandpack flooding experiments. The nanoparticles-$C_{12}E_{23}$ demonstrated high salinity and temperature tolerance, with superior profile control and water blocking impacts, enhancing the recovery factor of oil by 20.1% after water flooding. These recent research were limited to either one type of nanoparticles or surfactants. Static and dynamic experiments for evaluating the performance of different nanoparticles and surfactants on CO_2 foam stabilization at subcritical and supercritical conditions have not been comprehensively conducted.

Despite the previous investigations of the influence of different factors on stability and mobility control of nanoparticles-surfactant stabilized foam, optimal conditions for attaining maximum foam generation and stability is not yet clear. Performance of nanoparticles-surfactant stabilized CO_2 foam at harsh reservoir conditions of high temperature, salinity and presence of oil require further extensive studies. In most of the previous studies, the best performing nanoparticles/surfactants are selected at the screening stage before conducting further foam stability tests through static stability experiments conducted at room condition and absence of oil. At realistic reservoir conditions, stable foams are expected to be generated in presence of high proportion of water to oil at elevated temperature.

Nanoparticles/surfactants screening experiments conducted at ambient conditions in absence of oil is not a true representation of actual foam performance at downhole conditions. There is significant difference in foam performance at ambient conditions, and at high temperature and presence of high proportion of water–oil ratio [22]. Until now, the conditions for the optimal generation and stability of nanoparticles-surfactant CO_2 foam are not clearly understood. CO_2 can exist at subcritical and supercritical condition, depending on the prevailing temperature and pressure. CO_2 behaves as gas at 273.15 K, and 14.5 psi but exist as supercritical fluid, adopting properties midway between gas and liquid, at its critical temperature and pressure (31.0 °C, 1,070 psi). The stability of CO_2 foam at its supercritical conditions is essential for successful field applications.

In this study, dynamic foam stability experiments were conducted using formulation turbiscan at high temperature and presence of oil, to screen three different surfactants and five different nanoparticles. The best performing nanoparticles and surfactant were selected at the screening stage before conducting further foam stability tests to compare the performance of CO_2 foam at sub-critical and super-critical conditions. Foam stability at the screening stage were evaluated from turbiscan stability index, backscattering and transmission profile, values of entering coefficient (E), spreading coefficient (S) and Lamella number (L). CO_2 foam at sub-critical and super-critical conditions were compared as a function of varying concentration of nanoparticles, oil types and salinity. Stability was evaluated from normalize foam height, microscopic images, as well as mobility reduction factor.

Formulation turbiscan used for dynamic foam stability screening experiments at high temperature and oil presence in this study has numerous benefits. The stability can be monitored for longer period at high temperature. The multiple light scattering detection method permits separate investigation of different mechanisms that influences foam/emulsion decay such as Oswald ripening, sedimentation, drainage, as well as coalescence in evaluating the foam stability in water-liquid emulsions [31,32]. The techniques have been applied for estimating dynamic foam stability in previous research [26–30].

2. Experimental

2.1. Materials

The triton X-100, cetyltrimethylammonium bromide, as well as sodium dodecyl sulfate were the surfactants used for the experiments. The TX 100, CTAB and SDS were bought from Merck Sdn. Bhd, Across Organics, and Sigma-Aldrich Sdn. Bhd. Malaysia respectively. They were more than 99% pure. Salinity effect on foam stability was explored with sodium chloride (laboratory grade) supplied by Merck Millipore. The carbon dioxide (more than 99% pure) for generating the foam was purchased from MMIG (Mega Mount Industrial Gases) Sdn. Bhd. Malaysia. Influence of oil on foam properties was studied with Normal hexadecane ($C_{16}H_{34}$), decane ($C_{10}H_{22}$), paraffin and crude oil. The n-decane, n-hexadecane, as well as paraffin oil was supplied by Sigma Aldrich, while the crude oil is a West Lutong Crude from Sarawak oilfield, Malaysia. Brookfield RST rheometer was used to determine the oil viscosities while pycnometer and density meter was used to measure the densities of the oil. The oil properties and the properties of the nanoparticles used for this research are shown in Table 1 and Table 2 respectively.

2.2. Methodology

2.2.1. Preparation of surfactant and nanoparticles-surfactant solutions

Solutions of solid surfactant samples were prepared via dispersion of the desired mass of the surfactant (in wt.%) into brine or deionized water solutions. The brine solutions were prepared by weighing the required grams of NaCl salts into the deionized water. Magnetic stirrer and mixer were used for dispersing the solid surfactant and salt in the brine/deionized water solutions. Desired concentration of liquid surfactant (TX100 solutions) were obtained from the dilutions of the standard solutions made from stock solutions. For nanoparticles/surfactant dispersions, the preferred quantity of nanoparticles and surfactants were weighed out in grams and dissolved into the brine/water solutions. Subsequently, the nanoparticles-surfactant solutions were magnetically stirred for half an hour and sonicated using QSonica (model: Q500 sonicator) operated at 500 W and 20 kHz frequency.

Table 1
Oil types, suppliers, viscosities and densities.

Oil types	Suppliers	viscosity	Density
N-decane ($C_{10}H_{22}$)	Sigma Aldrich Co., Ltd.	0.93 cp	0.73 g/cm^3
N-hexadecane ($C_{16}H_{34}$)	Sigma Aldrich Co., Ltd.	3.33 cp	0.77 g/cm^3
paraffin oil	Sigma Aldrich Co., Ltd.	21 cp	0.85 g/cm^3
Crude oil	West Lutong Crude	10 cp	0.83 g/cm^3

2.2.2. CO_2 foam generation and stability at subcritical condition

The CO_2 foam at subcritical condition was produced by dispersing CO_2 gas at flowrate of 0.05 ml/seconds via gas diffuser (100 μm diameter) through foam column (with height 50 cm and internal diameter of 5 cm) into the 100 ml foaming solution. The foam was generated for 300 s and the top was covered instantly the gas sparging was terminated to minimize the impact of environmental humidity. The CO_2 foamability and stability were characterized by the optimum height attained in the foam column, and the collapse rate of the foam after every 180 s. The foam stability was estimated from plot of normalized height versus time [14,33]. The normalized height is expressed as follows:

$$\text{Normalized height} = \frac{\textit{Foam height at present time } t}{\textit{Initial foam height } (\textit{when } t = 0)} \quad (1)$$

2.2.3. CO_2 foamability and stability at supercritical condition

Schematic of the apparatus used for CO_2 foam dynamic generation and stability experiments at supercritical condition is presented in Fig. 1. To generate the foam, the CO_2 accumulator was filled with the CO_2 while the ISCO pump was loaded with aqueous dispersion ensuring that there was no trapped air in the injection line and ISCO pump cylinder. The CO_2 was introduced to the system via CO_2 injection valve at constant injection rate of 6 ml/min. The supercritical CO_2 and the foaming dispersions are mixed within the glass-bead packed column (GBPC) by a strong shearing energy, forcing the adsorption of nanoparticles at the CO_2-water interface. The differential pressure transducer (Honeywell STD770) connected to a measurement computing system, USB-1608G data acquisition (DAQ), measured the pressure drop across the GBPC. The pressure drop was recorded via the Lab VIEW software.

The foam flowed into a quartz observation tube after leaving the GBPC. The injection of CO_2 into the system was sustained till the breakthrough of CO_2 in the view cell. The foam morphology and stability with time were observed in the observation tube. The entire flow line was coiled with heating tape that can increase the temperature of the system up to 60 °C. The pressure was maintained at 1500 psig throughout the experiments. The foam image in the view cell was captured with camera every 3 min interval to record the foam collapse rate with time.

2.2.4. Foam dynamic stability evaluation through optical technique

The produced foam dynamic stability in presence of high volume of oil (30 wt% of normal (hexadecane oil) at 80 °C was characterized with TURBISCAN Lab Expert Stability Analyser (manufactured by Formulation, France) using dynamic light scattering basis as shown in Fig. 2. The sample vials containing 50 ml of generated foam at different concentrations were positioned in the Formulation TURBISCAN for further analysis. The stability of the foam was estimated from TSI (Turbiscan stability index), backscattering and transmission profiles. Stability was monitored

Table 2
Nanoparticles types and properties.

Nanoparticles	Suppliers	Properties		
		Purity	Specific SurfaceArea (SSA)	Size
Titanium dioxide (TiO_2) nanoparticles	Sky Spring Inc. USA	99.9%	200–240 m^2/g	18 nm
Silicon dioxide (SiO_2) nanoparticles	US Research Nanomaterials Inc. USA	99.5%	170–200 m^2/g	5–20 nm
Copper (II) oxide (CuO) nanoparticles	Sky Spring Inc. USA	99%	20 m^2/g	40 nm
Aluminium (Al_2O_3) oxide nanoparticles	Sky Spring Inc. USA	>99%	38 m^2/g	20 nm
Multi-walled carbon nanotubes	Chengdu Organic Chemicals Co. Ltd. China	>98%	350 m^2/g	length (0.5–2 μm), outer diameter (<8 nm) and internal diameter (<2–5 nm)

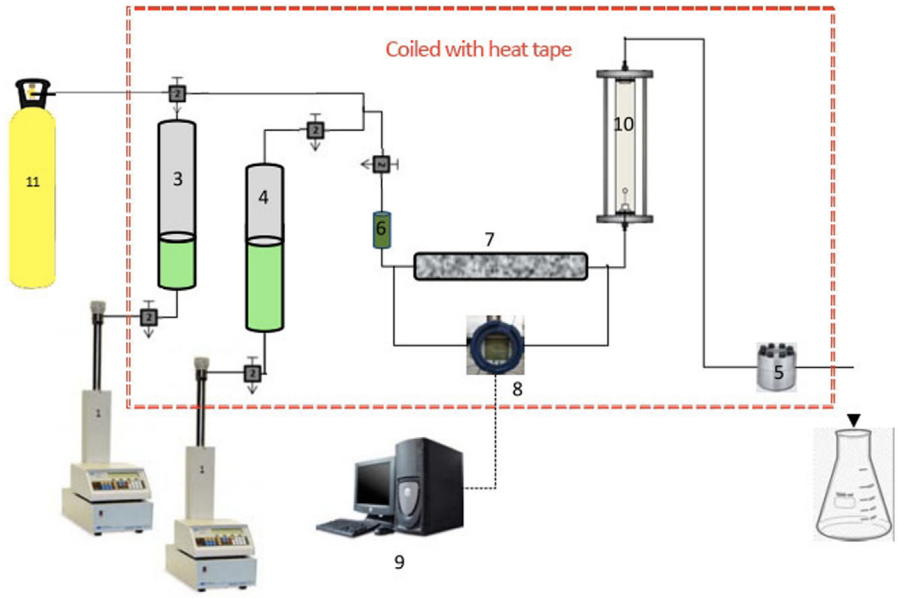

Fig. 1. Pictorial representation of experimental set-up for evaluation of CO_2 foam generation and stability at supercritical condition. The experimental set-up consists of (1) ISCO pump (2) Swagelok valves (3) CO_2 accumulator (4) Foaming solutions/brine accumulator (5) backpressure regulator (6) In-line filter (0.5 μm) (7) GBPC (8) Pressure transducer (9) data acquisition system (10) View cell and (11) CO_2 tank.

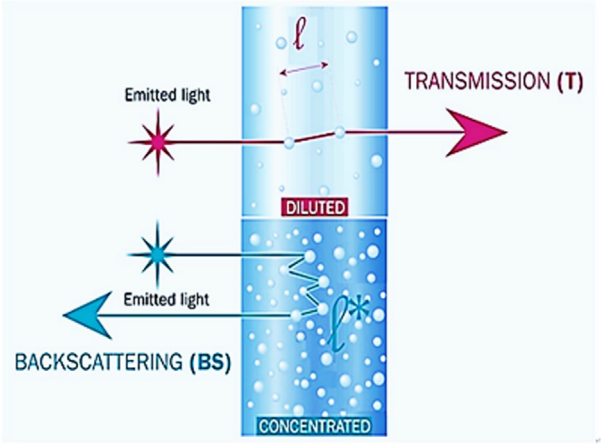

Fig. 2. Formulation TURBISCAN Working principle [39,40]

for 12 h at 80 °C by samples scans at 880 nm every 120 s in the Formulation Turbiscan. The value of TSI increases with the increasing bubbles coalescence and coarsening process. Higher TSI value signifies unstable system and lower foam stability.

The analyzer detect the BS as well as transmission light intensity of a pulsed near infra-red-light source ($\lambda = 880nm$) (via) across the sample. The principle is described in Fig. 2

$$BS \approx \frac{1}{\sqrt{\lambda^{\star}}} \tag{2}$$

$$\lambda^{\star}\varphi, d) = \frac{2d}{3\varphi(1-g)Q_s} \tag{3}$$

In Eq. (2), the mean free path of photon in the dispersed phase is represented by $\lambda^{\star}$, d is the particle diameter/size, the dispersion phase volume concentration is φ, Q_s and g are the optical parameters from Mie theory. Each scan of a particular measurement is compared to the preceding one, on designated height, and the outcome is divided by total height chosen, so as obtain a result that does not depend on amount of measuring cell content. This principle is employed in calculation of TSI as expressed in Eq. (4) [34–38]

$$TSI = \frac{\sum_h |scan_i(\mathrm{h}) - scan_{i-1}(h)|}{H} \tag{4}$$

Where *TSI*: represents the Turbiscan Stability Index,

H : represents the total height of the sample from base of the cell unto the meniscus),

h :is the selected height of the sample respectively.

$scan_{i-1}(h)$: is intensity of the scanning light at time is $i-1$, and height, h.

i is the time from 1 to k,

$$\mathrm{k} = total\ time/scan\ speed \tag{5}$$

2.2.5. Analysis of the foam microscopic images

The characterization of the size distribution of foam, and the thickness of the foam lamellas was conducted with Leica EZ4 HD microscope. Micro-bubbles samples were placed on a microscope slide and enclosed with microscope cover slip for bubbles and droplet structural analysis under the microscope. The alterations of the morphology of the generated bubbles and change in lamellae thickness with time were inspected with Olympus IX53 microscope. Confocal laser scanning microscopy Zeiss, (LSM 800) was used for investigating the distributions of the nanoparticles in the oil–water and gas–liquid interface. Three dimension and Topography analysis of the micro-bubbles was conducted with MMS version 7 (Mountain Map software).

2.2.6. Surface/Interfacial tension measurement

The measurement of water–gas, water–oil and the oil–gas interfacial tension surface and interfacial tension for calculation of entering coefficient (E), spreading coefficient (S), and the lamellae number (L) was conducted through Pendant drop method using Krüss drop shape analyzer (DSA 25 and DSA 100) and spinning drop interfacial tensiometer. The experimental details have been reported in our previous studies [11, 13].

3. Results and discussion

Successful application of foam for gas mobility control depends on foam generation and stability at high temperature and oil presence. Several literatures have shown that the viscoelasticity and interfacial stabilizing capacity of conventional foaming agent increased in presence of nanoparticles. However, most of foam stability tests at the screening stage are rarely conducted at dynamic condition of high temperature and presence of oil, thus most reported results and not representative of foam performance at reservoir conditions.

3.1. Screening of best performing nanoparticles and surfactants via dynamic tests

To select the best performing nanoparticles and surfactant for further foam stability experiments, nanoparticles-foam stability was investigated at the screening stage through light-scattering detection techniques. The method encompasses the processes of sedimentation, drainage, coarsening, as well as coalescence in determining the dynamic stability of foam. Different concentration of nanoparticles was introduced into the conventional foaming solutions, and foam stability were evaluated from transmission and back-scattered profiles, as well as the TSI. Afterward interfacial tension analysis was conducted to calculate entering coefficient (E), spreading coefficient (S), and the lamellae number. The nanoparticles and surfactant that most produced the most stable foams were then selected for foam stability tests at sub-critical and supercritical conditions.

To stimulate the actual downhole conditions at the screening stages, foam was generated in presence of 30% of hexadecane oil and then loaded into the formulation Turbiscan to study the foam stability at the dynamic conditions. Small value of turbiscan stability index (TSI) was taken as actual indication of the foam high stability. Influence of surfactant type, nanoparticles type and nanoparticles concentration were investigated. Fluorescence microscopy of foams images were obtained to elucidate the mechanisms of foam stabilization. Constant SDS concentration (0.5 wt%) as well as 0.1 wt% of TX100 and CTAB, representing significant values above the surfactants CMC were used for the experiments.

Result of the dynamic changes in foam stability at 80 °C investigated for 12 h via multiple light scattering method are presented in Fig. S1 (supporting information). The foams were generated using 0.5 wt% concentration of nanoparticles. The colour of the spectra is an indication of time in backscattering (BS) and the transmission (T) light intensity profiles of the foam stabilized by different nanoparticles and surfactant types presented in Fig. S1 (supporting information)**.** In previous studies, increasing transmission is usually attributed to quicker rate of liquid drainage whereas decreasing backscattering is an indication of film thinning and bubbles coalescence [26,30]**.** The decreasing transmission intensity at the base of the sample bottles is an indication of the extent of liquid drainage from foam lamella [26,30].

In Fig. S1 (supporting information)**,** almost zero percent (%) transmission was observed in transmission intensity profiles of SiO_2-CTAB and carbon nanotubes-CTAB (CN-CTAB) stabilized foams (Fig. S1a and S1e). The low transmission intensity at the bottom of samples height is an indication of the formation of compacted foam consisting of several bubbles per unit area (higher bubble density). Foam stability can also be attributed to higher backscattering intensity resulting from longer BS light scattering pathway. However, liquid drainage and gas diffusion from smaller bubbles into larger bubbles, at high temperature resulted in faster bubbles coalescence. Hence, backscattering (BS) reduces due to shorter BS light pathway whereas transmission (T) increases [26,30]. Fig. S1 (a, d and e) clearly showed that SiO_2-stabilized CUO-stabilized and carbon nanotubes-stabilized foams were most stable whereas Al_2O_3-stabilized and TiO_2-stabilized foams were the least stable Fig. S1(b and c). The presence of nanosilica and carbon-nanotubes in the CTAB solutions increases the interfacial energy, thus delayed the drainage of liquid from foam films as well as bubbles coalescence and coarsening.

3.1.1. Surfactant types screening

In consistent with the backscattering (BS) and the transmission (T) light intensity profiles, the plots of TSI against time presented in Fig. 3 plainly revealed that high temperature and high volume of oil rendered the foam unstable in presence of all investigated surfactants. The values of TSI were generally very high because increased temperature decreases CO_2 density at isobaric condition. Temperature weakened the surfactants solute–solute interaction, resulting in random movement of the solvent CO_2 and nanoparticles-surfactant molecules. Low CO_2 density at high temperature will also result in low molecular packing density of adsorption layer and increases the movement of nanoparticles-surfactant complex at foam lamellae, resulting in higher liquid drainage and faster bubble coalescence [41]**.**

Within the first 3 h, TX100-based foam demonstrated the highest stability (lowest TSI), due the greater tendency of TX100 to cause lowest reduction in oil–water interfacial tension compared to SDS and CTAB [15]. This suggests that TX100 has the best foam generation capacity among the surfactants. However, after 3 h, the plotted graphs showed that CTAB-generated foam displayed the lowest TSI (50%) and highest stability in comparison to TX100-foam (with TSI of 66.9%). The high durability of CTAB-stabilized foam resulted from the substantial self-aggregation properties of molecules of CTAB as a result of ample presence of carbon-atoms in CTAB tail, promoting surfactant molecules aggregation at interface [42]. After 9 h, the CTAB and SDS demonstrated almost equal stability as the TSI of SDS-foam and CTAB-foam remained constant at 50%.

3.1.2. Nanoparticles types screening

Largely, smaller values of TSI were exhibited by the nanoparticles-surfactant stabilized foam compared to the surfactant foam, signifying that these foams were thermally stable compared to the conventional foams (Fig. 4). The thermal dynamic stability of nanoparticles-surfactant foams arises from the nanoparticle's adsorption, as well as agglomeration on the bubble's surfaces [43]. This incident resulted in the formation of colloidal armour of dense films at the foam lamellae to prevent bubble decay.

Among all the nanoparticles types, carbon nanotubes produced the lowest TSI, followed by SiO_2 nanoparticles. The increasing sta-

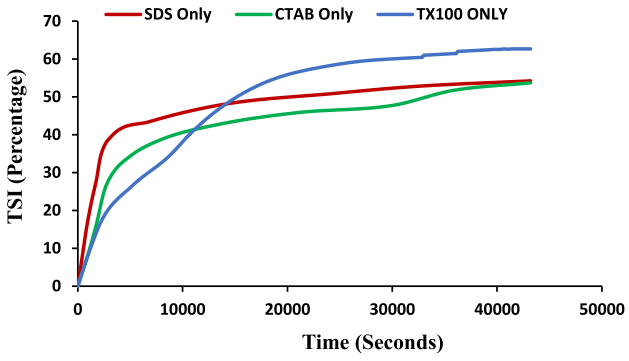

Fig. 3. TSI of surfactant-stabilized foam in presence of 30 wt% Hexadecane at 80 °C.

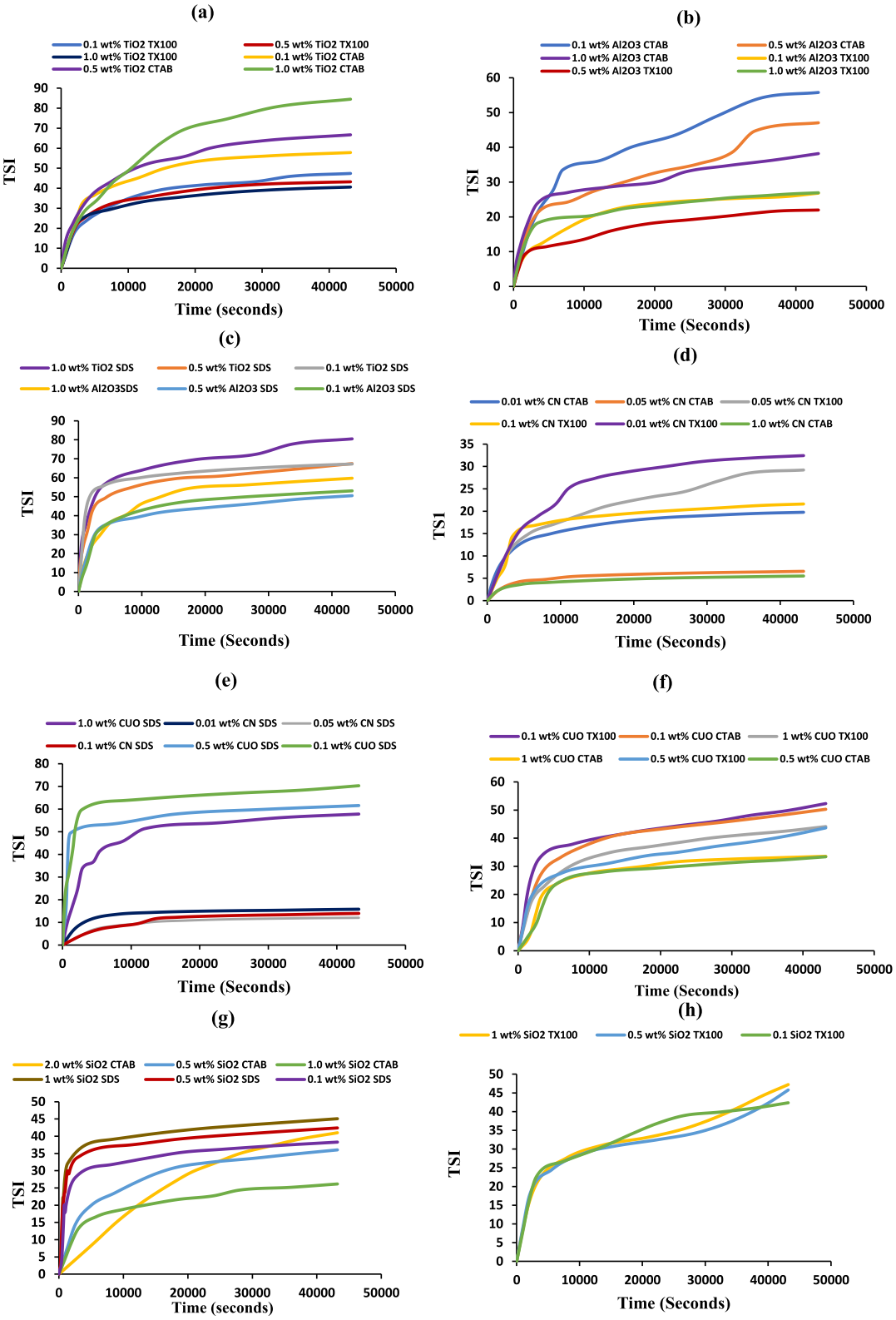

Fig. 4. TSI of nanoparticles-surfactant stabilized foam in presence of 30 wt% hexadecane at 80 °C.

bility (decreasing TSI) is in following order: carbon-nanotubes> SiO_2 >CUO > Al_2O_3> TiO_2. Critical inspection of the plotted graphs in Fig. 4 revealed that regardless of the surfactant type, the TSI of the foams stabilized by only surfactants, as well as foams stabilized by TiO_2 and Al_2O_3 nanoparticles exhibited highest tendency to increase indefinitely with time (Fig. 4a–c). But the TSI of foams stabilized by carbon nanotubes, SiO_2 and CUO nanoparticles remained constant after some time Fig. 4(d–h). These results suggest that the

decaying process of surfactant-stabilized foams, as well as TiO_2 and Al_2O_3-stabilized foams could get worse with time in actual reservoir conditions.

Formation of very stable carbon nanotubes-stabilized and SiO_2-stabilized foam in presence of high ratio of oil to water at elevated temperature arises from propitious orientation of particles at water-hexadecane-gas interface. When high ratio of oil to water is present in aqueous medium along with the foaming agents, the foam stability depends on the presence of the foaming/stabilizing agents at gas–liquid as well as oil–water interfaces [22]**.** Carbon nanotubes have been identified as stable emulsion stabilizers from previous studies because of the favourable alignment of the nanomaterials at interface of oil and water [44].

3.1.3. Nanoparticles concentration screening

The concentration of all nanoparticles was varied between 0.1 and 1.0 wt%, to investigate impact of nanoparticles concentration on foam stability. But concentration of 0.01–0.1 wt% was used for carbon nanotubes because of their less dispersity in bulk/surfactant solutions [45]. Fig. 4 clearly showed that as the nanoparticles concentration increased from 0.1 to 1.0 wt%, the foam stability also increases. For instance, after 12 h, SiO_2 in CTAB solution decreased the TSI from 53.72% to 36.04% and 26.15% with increasing nanosilica concentration from 0.5% − 1 wt% respectively (Fig. 4g). Similarly, the TSI of TX100-foam reduced from 66.90% to approximately 22% with 0.5 wt% nano-alumina in surfactant solution (Fig. 4b). The highest concentration of carbon nanotubes (0.1 wt%) considerably reduced the TSI of the foam generated with CTAB and SDS from 50% to 5.5% and 13.92% respectively (Fig. 4d and e).

Generally, lowest TSI and best foam stability was achieved when the nanoparticles concentration varied between 0.5 and 1 wt% concentration. For carbon-nanotubes, the plotted graphs generally showed that TSI values decreased significantly with the increasing carbon-nanotubes concentration in surfactant solution. The extent of adsorption of nanoparticles-surfactant complex, as well as the molecules accumulation at foam lamellae is expected to increase as the particle's concentration increases until the bubble interfaces are impeccably shielded from film-thinning, coalescence and coarsening [46]. Moreover, Ostwald ripening can be reduced at higher nanoparticles concentrations, because the osmotic pressure acting within the bubbles balances the Laplace pressure variations [47].

Whenever the nanoparticles concentration is too low, there is insufficient quantity of nanoparticles-surfactant (nano-surfactant) complex at foam lamellae. This incident will result in lower rate of nano-surfactants species adsorption, as well as aggregation at gas–water interface. This study suggest that ample quantity of nanoparticles is require for absolute fortification of bubble's surfaces from film thinning and decay.

3.2. Screening of best performing nanoparticles and surfactants via E, S and L

To confirm the best performing nanoparticles and surfactants for further foam stability experiments. Foam-oil interaction was systematically evaluated from three parameters (models) that are frequently engaged in previous studies. These models are entering coefficient (E), spreading coefficient (S), and bridging coefficient (B). They are mathematically expressed as [48,49]:

$$E = \sigma_{w/g} + \sigma_{w/o} - \sigma_{o/g} \tag{6}$$

$$S = \sigma_{w/g} - \sigma_{w/o} - \sigma_{o/g} \tag{7}$$

$$B = {\sigma_{w/g}}^2 + {\sigma_{w/o}}^2 - {\sigma_{o/g}}^2 \tag{8}$$

Interfacial tension is represented by σ while the subscript o stands for oil, w stands for water (foaming agent) and g for gas respectively.$\sigma_{w/g}$,$\sigma_{w/o}$, and $\sigma_{o/g}$ are the water–gas, water–oil and the oil–gas interfacial tension respectively.

Foam stability is defined by negative entering coefficient (E), suggesting that the oil droplet resides at the water phase, and will only be able to invades the gas–liquid interface of the foam whenever entering coefficient becomes greater than zero ($E > 0$). Likewise, spreading of oil becomes favourable whenever spreading coefficient (S) is positive. Oil spread at the gas–water interface does not occur if S is negative [48,49]. Stable foam films are indicated by the negative value of bridging coefficient (B), while the unstable foam film is represented by $B \geq 0$. Influence of hydrocarbons on the lamella of foam can also be quantified by the Lamella number (L) represented by [50]

$$\mathrm{L} = 0.15\frac{\sigma_{w/g}}{\sigma_{w/o}} \tag{9}$$

Highly durable foams are signified by $\mathrm{L} < 1$,as well as negative values of entering (E) and spreading (S) coefficient. Unstable foams are signified by positive values of entering (E), and spreading (S) coefficient, as well as $\mathrm{L} > 7$. The conditions for foam to be described as moderate stable are positive value of entering (E) coefficient, negative value of spreading (S) coefficient, and $1 < L < 7$ [48,49]. The measured and calculated parameters are presented in Table S1 (Supporting information). Positive values of entering coefficient (E) were obtained for all investigated cases in this study, showing that the presence of nanoparticles did not prevent the invasion of interface between the liquid and the gas by the oil. However, negative values of spreading coefficients were obtained for most of the nanoparticles-surfactant foams while spreading (S) coefficients for all surfactant-stabilized foams were positive.

These results showed that the oil favourably dispersed at the gas–water interface of foams stabilized solely by the surfactants while nanoparticles adsorption and aggregation at the gas–liquid interface prevented oil spreads at the lamellae of nanoparticles-stabilized foam. The calculated values of lamellae number were all less than 7 whiles $\mathrm{L} < 1$ were obtained for the highly stable nanoparticles-surfactant stabilized foam. It can be inferred from Table S1 (Supporting information) that nanoparticles did not necessarily prevent the entering of oil into the gas–liquid interface but prevented the spreading of invaded oil by keeping the pseudo-emulsion films stable.

Table S1 (Supporting information) further confirmed that the most stable foams from the multiple light scattering and turbiscan stability index (TSI) demonstrated favourable spreading coefficient (S) and lamella number (L) compared to the least stable foam. For instance, SiO_2-SDS, SiO_2-TX100, CN-SDS and CN-CTAB spreading coefficient (S) were negative and the lamella number (L) were favourable for foam stability while only the TIO_2-SDS foam displayed negative spreading coefficient. The spreading coefficient of TIO_2-CTAB and TIO_2-TX100 and Al_2O_3/TX100 foams were all positive with lamellae number > 1, confirming that the foam stabilized by TiO_2 and Al_2O_3 nanoparticles were not as stable as carbon-nanotubes and nanosilica stabilized foams in presence of oil.

3.3. Screening of best performing nanoparticles and surfactants via static stability

Static stability experiments were further conducted to screen the best nanoparticles for further experiments. The least spreading coefficient and lowest lamella number were determined from interaction of nanoparticles-SDS mixtures with oil as shown in Table S1 (Supporting information). For instance, SiO_2-SDS foam has the lowest spreading coefficient −5.28 mN/m with lamella

number of 0.71, Al_2O_3-SDS foam has the spreading coefficient of −4.74 mN/m and lamella number of 0.39 while CN-SDS foam has the spreading coefficient of −3.47 mN/m and lamella number of 0.75. Further screen experiments were conducted using nanoparticles and SDS mixtures. Fig. 5 showed the plots of normalized height versus time for foam generated at 80 °C in absence of oil. The plotted graphs showed that CN-SDS foam with amazing dynamic stability in presence of oil has very poor stability in absence of oil while Al_2O_3-SDS foam with very poor durability in presence of oil has the best stability in absence of oil.

SiO_2-SDS foam showed consistent high static stability at 80 °C and dynamic stability in turbiscan at 80 °C and presence of hexadecane. The SiO_2-SDS foam also has the lowest spreading coefficient in presence of hexadecane oil and favourable lamellae number. Hence SiO_2-SDS foam will be chosen for further experiments to compare the performance of sub-critical and super-critical CO_2 foam in this study. We attributed the observed difference in static and dynamic foam stability in this study, to the influence of particles orientation at the gas–water interface of foam and oil–water interface formed in presence of oil. This assertion has been discussed in detail at "mechanistic investigation of foam stability in Section 4".

The high stability of SiO_2-SDS foam is confirmed by the microscopic image of the SiO_2-SDS foam lamellae presented in Fig. 6. Although the presence of hexadecane oil was observed at the foam lamellae, the pseudo-emulsion film remained stable, resisting oil spread, drainage and bubbles coarsening, because of their higher mechanical stamina impacted by the nanoparticles. The lamellae detachment and collapsing are prevented by nanoparticles adsorption at the lamellae which prevented drainage of the liquid from the foam films arising from gravity [6].

3.4. Comparison of CO_2 foam stability at sub-critical and supercritical conditions

SiO_2 nanoparticles and SDS surfactants were chosen for further foam stability tests to compare the foam performance at sub-critical and supercritical conditions. Although CN-CTAB foam demonstrated highest dynamic stability in turbiscan, their static stability was very poor. SiO_2-SDS foam showed lowest spreading coefficient and lamellae number in presence of oil, coupled with their moderate static and dynamic stability in turbiscan at 80 °C and oil presence. The stability of SiO_2-SDS foam at sub-critical and supercritical conditions were investigated as functions of varying nanoparticles, salinity and types of oil.

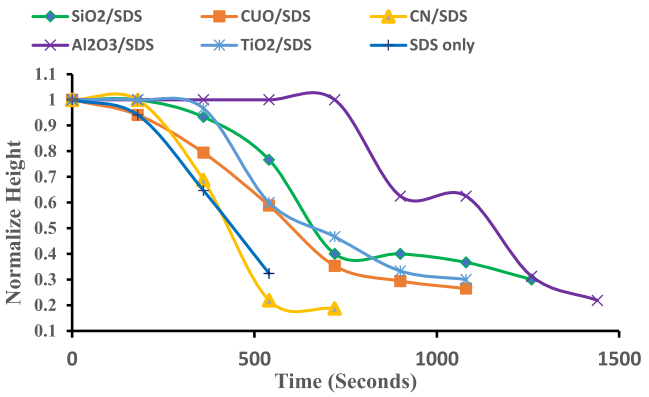

Fig. 5. Plots of normalize foam height versus time from the dynamic stability of nanoparticles-SDS foam at 80 °C in absence of oil. The foam was generated using 0.5 wt% SDS and 0.1 wt% for all nanoparticle's concentration.

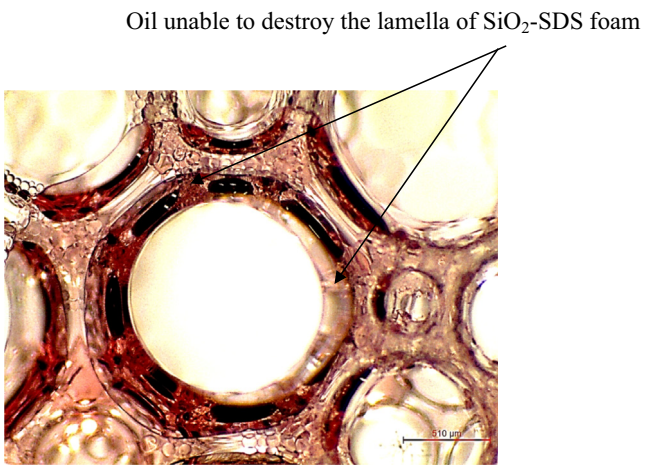

Fig. 6. Nanoparticles-surfactant foam lamellae showing that liquid drainage, as well as detachment and lamellae collapsing by hexadecane oil are delayed by nanoparticles. The foam was generated with 0.5 wt% SiO_2 and 0.5 wt% SDS.

3.4.1. Nanoparticles concentration effect on sub-critical and supercritical CO_2-foam

Nanosilica concentration impact on CO_2 foam stability was investigated at fixed concentration of SDS higher than CMC (0.5 wt%). The plots of normalize foam height against time at different nanoparticles concentration for sub-critical and supercritical CO_2 foam is presented in Fig. 7. Increasing nanoparticles concentration from 0 wt% – 2 wt% increased the stability of CO_2-foam generated at sub-critical condition (Fig. 7a). However, 0.5 wt% SiO_2 concentration was the most favourable for achieving maximum stability for super-critical CO_2 foam (Fig. 7b). When the nanoparticles concentration was increased beyond 0.5 wt%, the stability of super-critical CO_2 foam decreases (Fig. 7b). This study suggests the existence of ideal concentration for maximum stability of super-critical CO_2 foam.

There was no need to increase the nanoparticles concentration to highest concentration investigated at sub-critical condition (2.0 wt%) since the maximum supercritical CO_2 foam stability was attained at 0.5 wt%. Hence, 1.0 wt% SiO_2 concentration was the highest nanosilica concentration investigated at supercritical condition in this research. The supercritical CO_2 foam image in quartz tube presented in Fig. 8 further confirmed that 0.5 wt% SiO_2 shows better synergy with SDS compared to 0.6 wt% and 1.0 wt% SiO_2 at supercritical condition. There was almost an insignificant decrease in foam stability for almost 1 h. The foam height decreased by just 2 cm (from 15.50 cm to 13.50 cm) within 48 min between 12 min and 60 min.

The SDS surfactant molecules synergistically interacted with the SiO_2 nanoparticles to form a rigid armour structure at the thin liquid films that delayed film thinning and bubble coalescence as shown in Fig. 5 [24]. The existence of ideal concentration for utmost stability of the supercritical CO_2 foam can be attributed to rising density and increasing cohesive energy of the CO_2 at high pressure [41,51]. This incident favours the nanoparticles-surfactant interaction due to increasing hydrophobicity of the CO_2, thus expediting the entrenchment of nanoparticles-surfactants hydrocarbon tails into CO_2 phase.

The mobility of the supercritical CO_2 foam in porous media at different nanoparticles concentration was estimated using Eq. (10) [52]

$$\lambda = \frac{\left(\frac{Q}{A}\right)}{\left(\frac{\Delta P}{L}\right)} \tag{10}$$

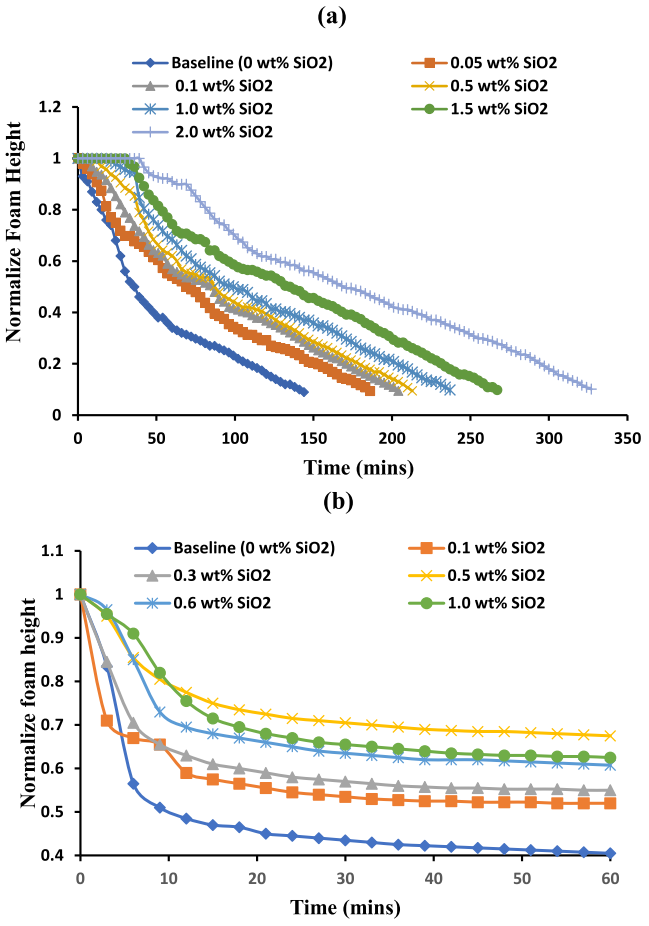

Fig. 7. Nanoparticles concentration effect on (a) Sub-critical CO_2 foam stability and (b) Super-critical CO_2 foam stability.

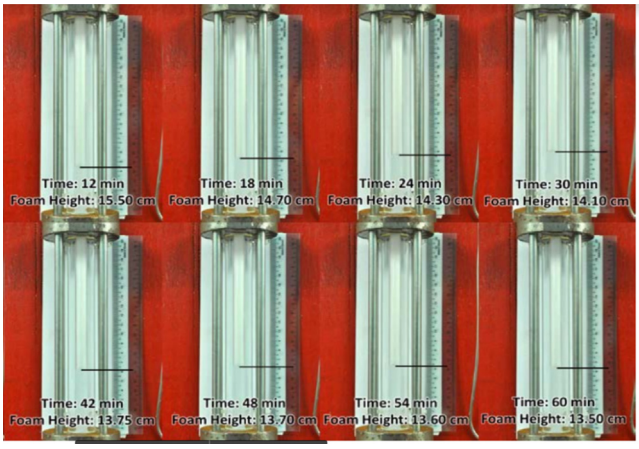

Fig. 8. Change in supercritical CO_2 foam height with time in quartz tube showing insignificant decrease in height within 60 min (the foam was generated with 0.5 wt % SiO_2 and 0.5 wt% SDS).

where A is the cross-sectional area of glass bead packed column (GBPC) obtained as 1.623 cm^2, L is the length of the GBPC (10 cm), Q is the volumetric flow rate (6 ml/min), λ is the foam mobility in mD/cP and ΔP is the pressure drop across GBPC in psi. The porosity of the glass bead was estimated as 34% while the permeability was determined as 60 Darcy.

The mobility reduction factor (MRF) or the foam resistance factor was subsequently calculated using Eq. (11), higher mobility reduction factor indicates lower reduction in foam mobility [52].

$$\text{MRF}, \gamma = \frac{\lambda_{\text{aqueous}-CO_2}}{\lambda_{\text{aqueous}-CO_2-\text{NPs}}} \tag{11}$$

Supercritical CO_2 foam static and dynamic stability were quite consistent. Pressure drops across GBPC demonstrated no noticeable variation as the SiO_2 concentration increased beyond 0.5 wt% SiO_2. The maximum pressure drops (Δp) was obtained as 22.548 psi with addition of 0.5 wt% SiO_2 to foam formulation. The Δp slightly increased to 22.603 psi and 22.708 psi when the concentration of the nanosilica increased to 0.6 and 1.0 wt% respectively. The pressure drops obtained in presence of 0.5, 0.6 and 1.0 wt% SiO_2 resulted in insignificant change in mobility and MRF as shown in Table 3. These results showed that there was no significant change in pressure drop, as well as the supercritical CO_2 foam mobility in porous media when the nanoparticles concentration exceeds 0.5 wt%.

The lower nanoparticles concentration required for attaining the maximum stability of CO_2 foam at the supercritical condition is due to response of CO_2 foam to pressure increase [51]. Previous studies have shown that CO_2 foam stability is enhanced at high pressure when surfactants with high hydrophile-lipophile balance (HLB) are used in foam generation [51]. At supercritical condition, the higher operation pressure (1500 psi) at constant temperature condition increased the CO_2 density and its cohesive energy density [51]. This incident increased the hydrophobicity of CO_2, consequently expediate the embedment of surfactants lipophilic groups (hydrocarbon tails) into CO_2 phase.

The higher interaction between the molecules of surfactants and CO_2 at high pressure of supercritical CO_2 foam is balanced by the strong hydrophilic heads of the SDS surfactant used in this study. Hence, maximum supercritical CO_2 foam stability was achieved with 0.5 wt% SiO_2. However, for the sub-critical CO_2 foam, the high hydrophilicity of SDS facilitated the embedment of hydrophilic groups (hydrophilic heads) of surfactants into the water phase. This interaction consequently increased CO_2 diffusion and water drainage through destabilization and thinning of the CO_2 foam liquid films. The stability of sub-critical CO_2 foam increased with increasing concentration of nanoparticles because high quantity of nanoparticles is required to attain maximum foam stability at sub-critical conditions. When the hydrophilic head of the surfactants are embedded into the water phase, the adsorbed surfactant molecules at the carbon-dioxide water interface are fewer resulting in poor foam stability [51].

3.4.2. Salinity effect on sub-critical and supercritical CO_2 foam stability

Fig. 9 shows the normalize height of the CO_2 foam generated at the subcritical (Fig. 9a) and supercritical conditions (Fig. 9b) at different salinity concentrations. The stability of sub-critical CO_2 foam was the best in absence of salt for the first 40 mins. After this time, the foam generated in presence of 2.0 wt% NaCl was better than the foam generated in absence of salt. Likewise, the super-critical CO_2 foam demonstrated good salt tolerance with the presence of 0.5 wt % as well as 2 wt% NaCl brine in SiO_2-SDS solutions. Just like the

Table 3
Mobility and mobility reduction factor (MRF) values at different SiO_2 concentration

Nanoparticles concentration	Mobility	Mobility Reduction Factor (MRF)
0.5 wt%	1.634×10^3 mD/cP	4.525
0.6 wt%	1.633×10^3 mD/cP	4.528
1.0 wt%	1.629×10^3 mD/cP	4.539

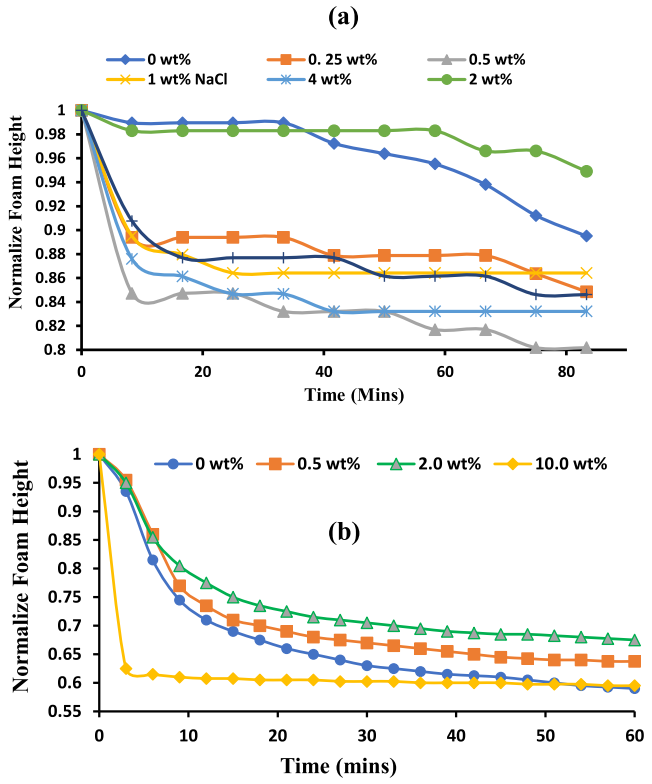

Fig. 9. Salinity effect on CO_2 foam stability at (a) sub-critical condition and (b) supercritical condition. The foam was generated with 0.5 wt% SDS and 0.5 wt% SiO_2.

case of sub-critical CO_2 foam, the super-critical CO_2 foam exhibited highest stability in presence of 2 wt% NaCl.

However, the bulk stability of the super-critical CO_2 foam reduced drastically when NaCl concentration increased to 10 wt %, suggesting the existence of optimum salt concentration for maximum stability of CO_2-foam generated at super-critical and sub-critical condition. The most stable sub-critical and super-critical CO_2 foams was generated in this study when 2 wt% NaCl was added to SiO_2-SDS solutions. The mobility of the super-critical CO_2 foam in glass bead packed column confirmed the foam bulk stability result. A closer inspection of the pressure drops during the foam propagation in the GBPC showed that the foam demonstrated increasing pressure drop with increasing NaCl concentration (Fig. 10).

The foam mobility was observed to reduce from approximately 2000 mD/cP in absence of salt to 1.633×10^3 mD/cP in presence of 2 wt% NaCl. The mobility further reduced to 1.545×10^3 mD/cP in presence of 10 wt% NaCl. The static and dynamic stability suggests that increasing salt concentration may not be detrimental to CO_2 foam stability. Instead the salt increased the foam stability until maximum salinity concentration was attained.

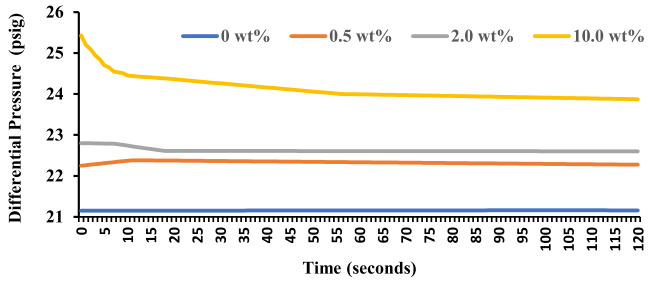

Fig.10. Differential pressure across GBPC at different salt concentrations.

The foam was generated with 0.5 wt% SDS and 0.5 wt% SiO_2.

The high foam stability can be attributed to increasing aggregation and optimum adsorption of nanoparticles-surfactant complex at foam lamella at high salinity condition. Since salts induces nanoparticles agglomeration, its presence in nanoparticles-surfactant solutions could facilitate nanoparticles-surfactant aggregation at gas–liquid interface [53]. This incident increased the interfacial activity of the surfactants and nanoparticles, resulting in high foamability and foam stability [54].

Increasing foam stability at high salinity conditions have been reported in literature [55–57]. Results of previous research showed that CO_2 foams apparent viscosity increased with increasing salinity concentrations from 0 to 22% total dissolved solids (TDS) while nanoparticles adsorption at CO_2-water interface was higher with presence of concentrated brine (15% TDS) in foaming solutions [56–59]. Xiao et al. [57] demonstrated that the apparent viscosity of CO_2 foams produced via the synergy of anionic surfactant and nanosilica rose from 0.02 to 0.1 cp when the concentration of salt was increased from 0 to 5 wt% NaCl. San et al. [59] observed that SiO_2-stabilized CO_2-foam produced in presence of 1.0 wt% NaCl attained total collapse after 7 days. But when the 10 wt% NaCl concentration was added into the foaming solution, less than 40% reduction in total CO_2-foam was noticed after 7 days. The foam mobility further decreased from 13.1 md/cp to 2.6 md/cp with increasing NaCl concentration from 1.0 to 10.0 wt% [59].

In the presence of salt, the screening of the charge on nanoparticles-surfactant complex aided in achievement of CO_2-philicity as well as migration of nanoparticles from the brine phase to CO_2-water interface to enhance foam stability [56–59]. More nanoparticles-surfactant molecules were adsorbed at the nanoparticles-CO_2 interface because the electrostatic repulsion among the nanoparticles-surfactant heads groups in aqueous solutions were reduced in presence of salt [57]. The increasing electrostatic attraction and the closer-packing of the adsorbed nanoparticles-surfactants molecules propelled the surface-active complex to the carbon dioxide-water interface to promote the foam stability [56–59]. Moreover, the screening electrostatic repulsion of the nanoparticles-surfactant head groups by the salts also assists in micelles formation, which impact the structural disjoining pressure. The change in formation of double layer, as well as screening of the repulsion between neighbouring charged silanol groups by the existing ions increased the hydrophobicity of silica nanoparticles, resulting in higher adsorption energy at the CO_2/brine interface [56–59].

However, Nanosilica agglomeration was observed when the concentration of NaCl was increased to 15 wt% in previous studies, suggesting that core plugging can occurred and optimum NaCl concentration exists for maximum foam stability at downhole conditions [59]. Likewise, whenever the salt concentration increases beyond the saturation point, the SDS-SiO_2 solution become supersaturated with excessive amounts of NaCl, resulting in the precipitations of surfactants, as well as nanoparticles-surfactant complex from the solutions. This process resulted in decreasing foam stability at NaCl concentration beyond 2 wt% observed in bulk stability experiments. At high NaCl concentrations, the precipitations of the surfactants from the foaming solutions can also obstructs the adsorption of surfactants onto the nanoparticles surface, consequently preventing nanoparticles-surfactant complex formation, adsorption, as well as agglomeration at foam lamellae.

3.4.3. Effect of types of oil on sub-critical and supercritical CO_2 foam stability

For investigating oil types effect on CO_2 foam stability. CO_2 foam was produced by the sparging of CO_2 into 50-cm cylindrical

glass column containing the foam solution. 5 ml of each oil was added to 100 ml of the foaming solution before the foam generation. Stability were estimated from normalize height, foam collapse in column with time, as well as the microscopic images. The plots of normalize height with respect to time presented in Fig. 11 showed that the foam was more stable when higher viscosity, higher density and high molecular weight oil was added into the foam dispersion in comparison to lower viscosity, lower density and lower molecular weight oil. In this study, the CO_2 foam was most stable in presence of paraffin (with highest viscosity) and was least stable in presence of n-decane oil (with lowest viscosity) as shown in Table 2. The CO_2 foam was also more durable in presence of n-hexadecane with molecular weight of $C_{16}H_{34}$ compared to n-decane with molecular weight of $C_{10}H_{22}$.

3.4.4. Effect of nanoparticles on foam stability in presence of oil

Results of this study showed that the foam collapse time was delayed by nanoparticles in presence of oil. In presence of paraffin, the total collapse time of CO_2 foam increased from 20 min to 160 min while in presence of n-decane, the CO_2 foam decay time increased from 16 min to 100 min when 1.0 wt% SiO_2 nanoparticles were added to the 0.5 wt% SDS solutions (Fig. 11).

The snapped images of the foam in foam column presented in Fig. S2 and Fig. S3 (Supporting information) showed consistent results with normalize foam height displayed in Fig. 11. The Figures showed that the nanoparticles-surfactant bubbles were finer, thicker, and denser due to slow rate of liquid drainage from bulk foam. The most striking observation from the foam decaying pattern in presence of oil in Fig. S2 and Fig. S3 (Supporting information) is the occurrence of irregular decay pattern with time for the SDS-stabilized bubbles. The collapse processes of the SDS-foam were in serrated pattern (Fig. S2) while uniform decay pattern was observed for SiO_2-SDS stabilized foam (Fig. S3). Non-uniform foam collapse profiles were also observed in presence of lower molecular weight, lower viscosity and density oil (decane oil) compared to foam generated in presence of high viscosity and density oil (paraffin oil).

The occurrence of irregular decay pattern for SDS-stabilized foam made it very difficult to reckon CO_2 foam stability from the visual inspection of foam decaying height with respect to time alone. Hence, the photomicrographs of the foams were complemented with normalize height for evaluation of the CO_2 foam-oil interaction. The results of this study generally confirmed that higher molecular weight, higher density, and high viscosity oils are less devastating to foam stability in comparison to oil with lower molecular weight, low density and viscosity [26,27]. The decane and paraffin oil distributions in the structure of

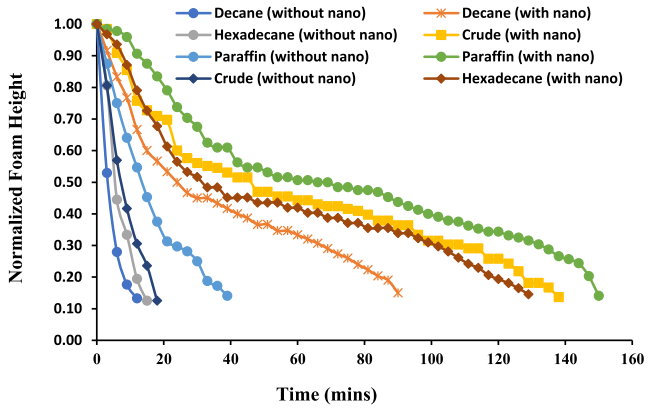

Fig. 11. The normalized height of SiO_2-SDS stabilized CO_2-foams geneated in presence of oil (foam formulation comprises of 0.5 wt% SDS and 1.0 wt% SiO_2).

nanoparticles-surfactant foam shown in Fig. S2 and Fig. S3 (Supporting information) showed the emulsification of oil to tiny droplets stuffing into foam thin-liquid films as well as Plateau borders to enhance the durability. However, the emulsified droplets hastily dispersed into the structure of SDS-foam to cause foam decay and coarsening. The structural arrangement of SiO_2-SDS bubbles permit oil accumulation within the Plateau borders and foam lamellae to enhance foam durability (Fig 12).

The microscopic images of CO_2 foam in presence of hexadecane oil with respected to time presented in Fig 12 showed the formation of high dense bubbles for both the SDS-stabilized foam and SiO_2-SDS CO_2 foam immediately after the foam generation, Initially, the bubble size distribution of the SDS-foam was also dominated by smaller and finer bubbles. These initial finer bubbles of the CO_2 foam can be attributed to higher interfacial activity and high foamability of surfactant and nanoparticles-surfactant due to their capacity to decrease surface-tension between CO_2 and brine [54].

Alzobaidi et al. [56] observed that the interfacial tension between CO_2 and concentrated brine (15% TDS) decreased from 25.0 mN/m to 12.7 mN/m in presence of nanosilica dispersions while Ibrahim and Nasr-El-Din, 2020 [60] found that interfacial tension between CO_2 and brine decreased from 20.5 mN/m to 14.7 mN/m in presence of anionic surfactant and further to 8.4 mN/m in presence of mixed system of anionic surfactant and SiO_2 nanoparticles.

The foam stabilized by only surfactant ultimately collapses faster while the initial swift collapse of the nanoparticles-surfactant enhanced foam was accompanied by a lengthy period of sustained durability. Most stable foams were produced through the synergy of SiO_2 and SDS because the SDS reduces the CO_2-water interfacial tension and equalizes the SiO_2 nanoparticles association with lipophilic- hydrophilic properties, resulting in sticking of nanosilica to CO_2-water interface [57].

Entering coefficient (E), spreading coefficient (S) and Lamella number (L) were calculated for foam-decane oil interaction Table S2 (supporting information) and compared with foam-hexadecane oil interaction Table S1 (supporting information). The calculated parameters clearly showed lower values of entering coefficient (E), spreading coefficient (S) and Lamella number (L) for CO_2 foam-hexadecane oil interaction compared to CO_2 foam-decane oil interaction, supporting the observation that lower molecular weight oils are more destructive to foam stability. Generally, oil with long chain, high viscosity, as well as high density have low propensity to become soluble into micelles [61,62].

The presence of oil with low micellar solubilization increases the forces of repulsion amid micelles (steric effects), consequently enhances the actual micellar bulk size and delays thinning of the foam's films [61,62]. Micrographs of the very stable foam (nanoparticles-surfactant foam and foam produced in presence of higher viscosity oil) showed the migration of droplets of oil from foam lamellae and subsequent collection in Plateau borders to retard thinning of the foam films (Fig 12 and Fig S3 (supporting information). Micrographs of the surfactant-stabilized foams and foam formed in presence of low viscosity and lower molecular alkanes oil (Fig S2, supporting information). showed quicker penetration of oil droplets into gas–liquid foam interface due to unstable pseudo-emulsion film [50].

Although the SiO_2-SDS bubbles were initially larger in size compared to SDS-stabilized bubbles (Fig. 12a-d), however, the SiO_2-SDS foam exhibited higher mechanical strength and high resistance to the destructive impact of oil compared to the conventional foams. The lamellae of SiO_2-SDS foams are more stable and resisted drainage and bubbles coarsening because of higher mechanical stamina impacted by the nanoparticles (Fig. 12e–l). The lamellae detachment and collapsing are prevented by the adsorption of

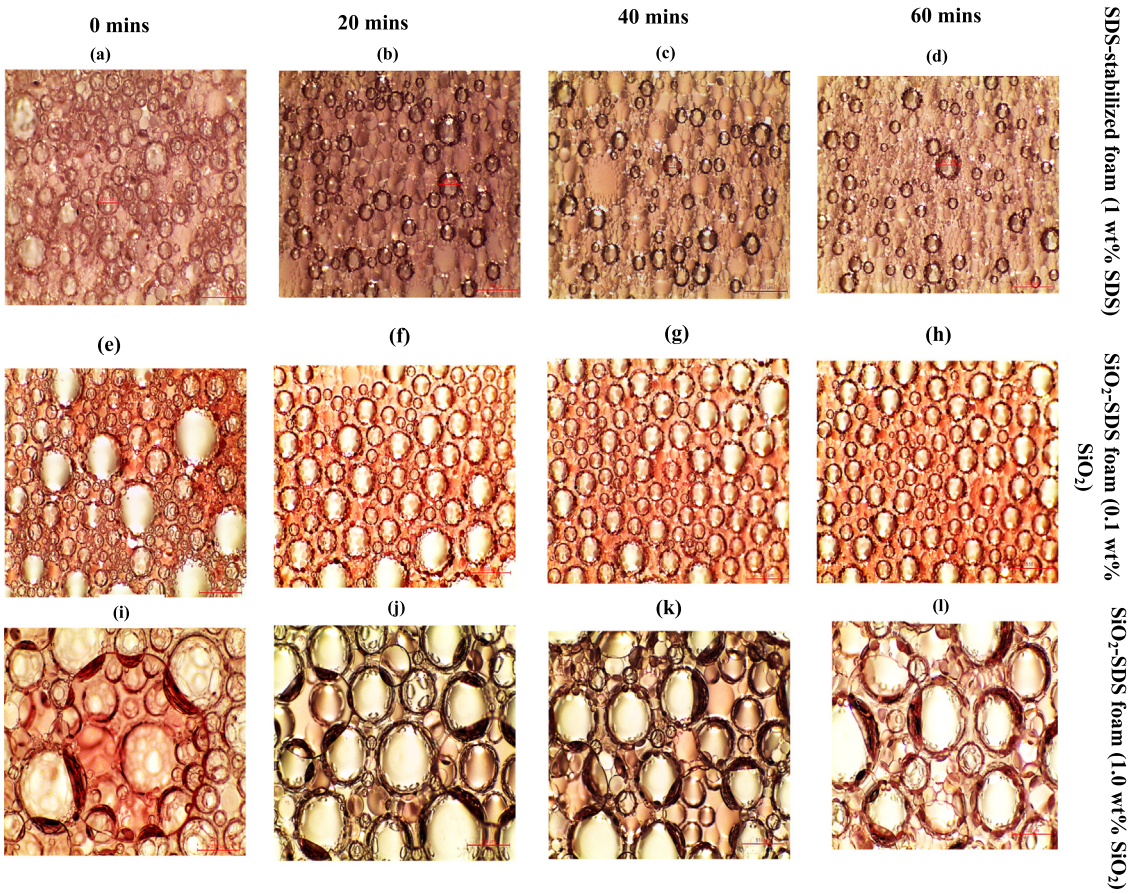

Fig.12. Microscopic images of SDS-foam (a–d) and SiO_2-SDS foam (e–l) showing that surfactant-foam could initially have smaller bubbles but collapses. The foam was generated in presence of hexadecane oil. 0.5 wt% SDS was used for SiO_2-SDS foam in (e–l).

nanoparticles at the gas–liquid interface which prevents liquid drainage from the foam films arising from gravity.

Results of this study (Fig.12) further suggest that foam stability cannot be infer from the generation of smaller and finer bubbles alone. Surfactants could induce higher foamability and produced initially smaller bubbles because of their higher interfacial activity more than nanoparticles. But they are unable to promote the eventual foam durability. Hence, their original smaller-sized bubbles collapse faster than the nanoparticles-stabilized bubbles. The durability of foam films determines the eventual stability of the generated foams. To elucidate the mechanisms of foam-oil interaction, it is recommended that the observation of bubbles collapse with time, be completed with the estimation of the entering and spreading of oil, as well as the detachment and destruction of foam lamella.

4. Microscopy investigation of mechanisms of foam stability

Mechanistic investigation revealed that the major difference between the surfactant- stabilized foam and nano-surfactant-stabilized foam is the change in lamellae thickness and microstructures of the generated bubbles with time. Though surfactant can produce finer bubbles at initial foam generation as observed during foam generation in oil, however SDS-stabilized foam collapsed faster and showed polyhedral shape with thinner lamellae (24.6 μm) with respect to time (Fig. 13a). Foams generated by SiO_2-SDS solutions were relatively stable with uniform or finer shape and denser lamellae (67.3 μm) (Fig. 13b).

The nanoparticles and surfactants screening experiments showed that TiO_2 and Al_2O_3 nanoparticles demonstrated high static stability in absence of oil at 80 °C but poor dynamic stability in presence of 30% hexadecane oil. Carbon nanotubes-stabilized foam exhibited low static stability but displayed amazing dynamic stability in oil presence. SiO_2 nanoparticle-stabilized foam demonstrated consistent static and dynamic stability with and without oil. To unravel the inconsistency in static and dynamic stability observed during the nanoparticles screening experiments, the mechanisms of foam stabilization in presence of higher oil volume was researched via confocal laser scanning microscopy. The micrographs from confocal showed that the structures of foams with high stability (low TSI) were of brighter fluorescence while least-stable foams have fainter structure.

Brighter fluorescence signified higher intensity of nanoparticles adsorption and arrangement at the lamellae. Generally, foams generated from nanosilica and surfactant formulation showed low TSI, brighter fluorescence and better stability. This observation is consistent with results of previous research [22,63]. Brighter fluorescence was observed for high stable foams and emulsions with fluorescence microscopy while fainter fluorescence are usually associated with low-stable foams and emulsions [22,63].

In the present study, when the foam was generated in presence of oil, the optical micrograph structures of CN-SDS and SiO_2-SDS foams showed brighter fluorescence Fig. S4 (supporting information) in comparison to that of TiO_2-SDS foam Fig. S5 (supporting information), because of the optimum adsorption of nano-surfactant complex at the bubbles surface. The foam destruction

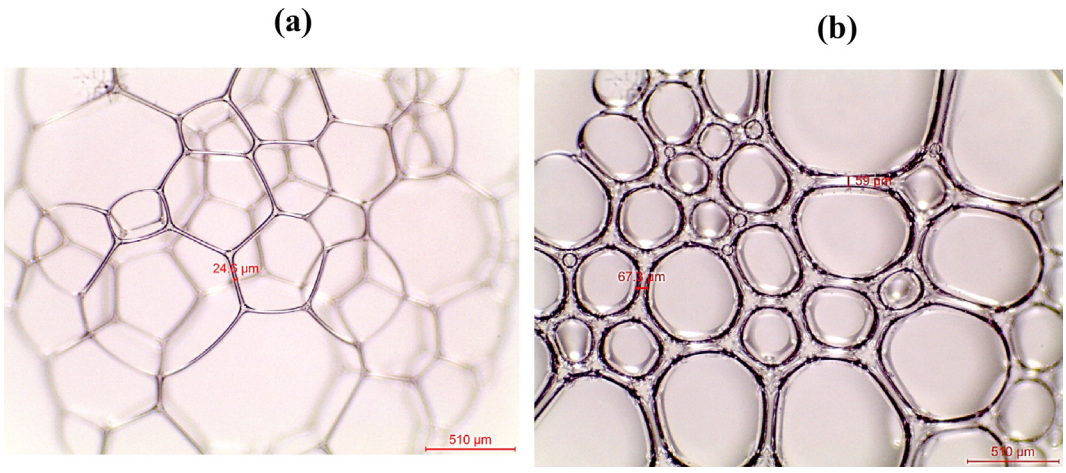

Fig.13. Morphology of (a) SDS-stabilized foam and (b) SiO_2-SDS stabilized foam. The foam in (a) was generated using 0.5 wt% SDS and foam in (b) with 0.5 wt% SDS and 1.0 wt % SiO_2.

at high temperature and presence of high volume of oil is prevented by the formation of interfacial colloidal armour. For the case of TiO_2-SDS stabilized foam with fainter fluorescence structure, the surface-active species were not sufficiently adsorbed at the interface. The stability of SiO_2-SDS stabilized foams was better because of sturdy cohesive intermolecular attraction within the similar charge molecules of surfactant and nanoparticles.

In the presence of high ratio of oil–water emulsions, the foam stability is a function of the surface-active complex alignment at oil–water and liquid–gas interfaces [22]**.** The microscopic images of carbon-nanotubes stabilized foam in Fig. S6 (supporting information), confirmed the presence of water–oil and liquid–gas interfaces in presence of oil. The three-dimensional (3D) imaging of the measured surfaces of foams stabilized by TiO_2-SDS, SiO_2-SDS, CN-SDS, as well as CN-CTAB presented in Fig. 14 showed the presence of aggregated particles, as well as poly-disperse droplet distribution at air–water and oil–water interface. The different colour of the spectra is an indication of particles aggregation intensity. The intensity of the particle's accumulation was higher at the interface for SiO_2-SDS foam (Fig. 14a) and carbon nanotubes-stabilized foam (Fig. 14c and 14d) compared to the titanium oxide nanoparticles-stabilized foams (Fig. 14b).

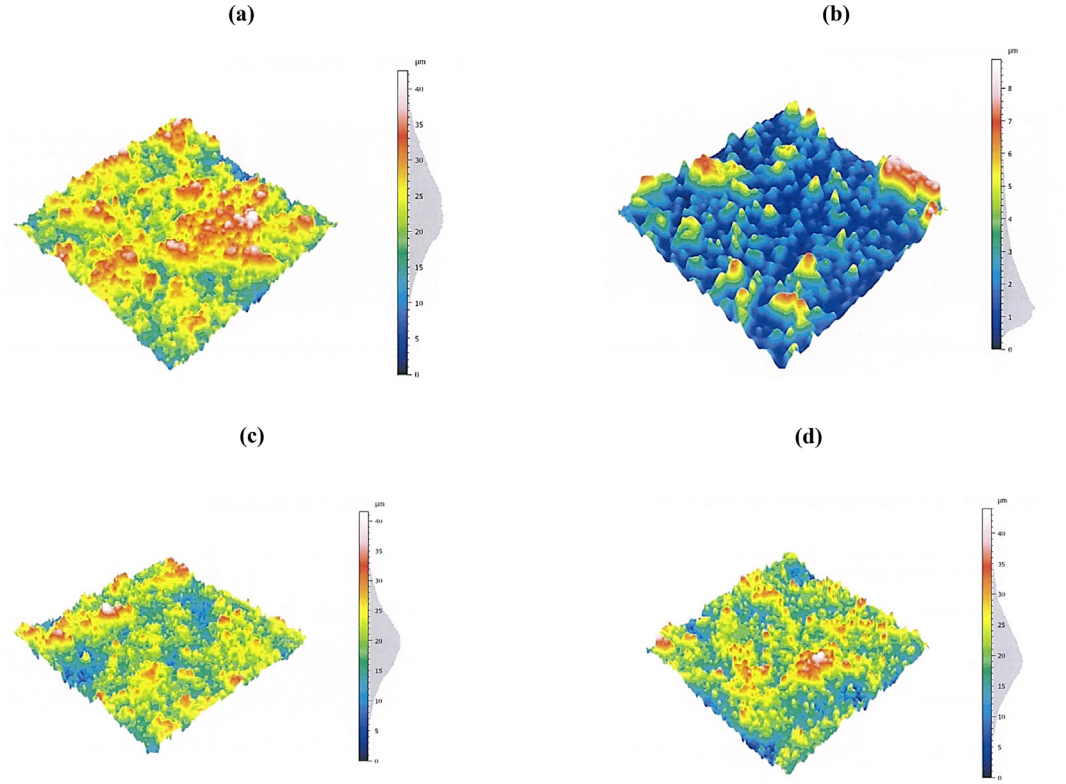

Fig. 14. Three-dimensional (3D) imaging for the measured surface of (a) SiO_2-SDS foam (b) TiO_2-SDS foam (c) CN-SDS foam and (d) CN-CTAB showing high density of aggregated particles at the surface of nanosilica and carbon nanotubes foam compared to TiO_2 foam. The foam was generated in presence of oil using 0.5 wt% SDS and 1.0 wt% nanoparticles concentration.

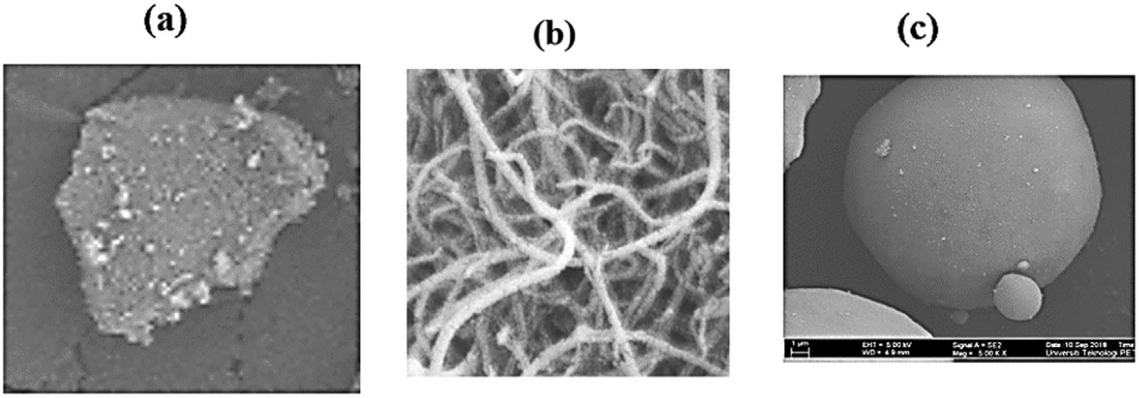

Fig. 15. Shape of (a) Al_2O_3 nanoparticles (b) carbon-nanotubes and (c) SiO_2 nanoparticles as obtained from variable pressure field emission scanning electron microscope.

In presence of high oil–water ratio, highest dynamic stability was obtained for the carbon nanotubes-stabilized and nanosilica-stabilized foams, compared with foam stabilized by other nanoparticles types because of favourable particles accumulation in the foam structure as observed in 3D surface imaging. The inclusion of carbon-nanotubes and nanosilica in the surfactant dispersions enhances the foam dynamic stability in presence of high volume of oil and water, due to favourable orientation of cylindrically carbon-nanotubes and perfectly spherical SiO_2 nanoparticles (Fig.15) to stabilize the interface between the water and hexadecane [44].

However, carbon-nanotubes stabilized foam with best stability in presence of oil showed very poor static stability in absence of oil while TIO_2 and Al_2O_3 nanoparticles with poorest stability in presence of oil showed good static stability in absence of oil. Only SiO_2 nanoparticles demonstrated consistent stability at static and dynamic conditions during the screening experiments. We inferred that cylindrical shaped carbon nanomaterials (Fig.15b) seem to be suited for stabilization of foam in presence of oil because they can be favourably oriented at oil–water interface. TiO_2 and Al_2O_3 nanoparticles can be most conveniently orientated at gas–water interface due to its irregular shape (Fig.15a) while almost spherical shaped SiO_2 nanoparticles comfortable aligned at both the oil–water and gas–liquid interface (Fig.15c).

In presence of high volume of oil and water, the SiO_2 nanoparticles effectively performed the dual functions of stabilizing the gas–liquid interface of foam, as well as the oil–water interface of the hexadecane and water in the emulsified network. Results of this study are consistent with literature, the findings of previous research established that SiO_2 nanoparticles and carbon nanotubes are novel emulsions stabilizers [44,64,65]. The perfectly spherical nature of nano-silica as well as the cylindrical structure of carbon-nanotubes are quite convenient for favourable positioning at oil–water interface to ensure foam stability in oil presence, compared to the other nanoparticles that were examined during the nanoparticles-screening experiments. Foam formulation from the combination of SDS and SiO_2 was quite stable in absence and presence of oil and demonstrated least spreading coefficients because of the existence of robust cohesive intermolecular interaction due to the similar charges of nanoparticles and surfactants molecules. Coupled with this effect, is the fact that the SiO_2 nanoparticles also adsorbed on the lamellae of the foam to prolong stability.

The three-dimensional (3D) imaging of the measured surfaces of foam generated in presence of oil during nanoparticles screening experiments displayed in Fig. 14, showed that strong steadying network with high bubble density and appropriate particles aggregation were formed, within the structure of very stable foams (carbon-nanotubes and SiO_2-stabilized foam) compared to the less durable foams (TiO_2 foam) in presence of oil. This kind of complex prevent thinning of the thin-liquid films and permit the migration of oil to Plateau borders to sustain foam stability at high temperature in presence of oil.

5. Conclusions and recommendations

This work is designed to identify the conditions for the optimum performance of CO_2 foam stabilized with synergy of surfactants and nanoparticles. Extensive static and dynamic foam stability experiments were conducted at 80 °C and presence of 30 vol% hexadecane oil using turbiscan, to screen different surfactants and nanoparticles. The best performing nanoparticles and surfactant were then selected at the screening stage for further foam stability tests to compare the performance of CO_2 foam at sub-critical and super-critical conditions.

The following conclusions and recommendations are drawn from the study.

1. Foams stabilized by cylindrically oriented multiwalled carbon nanotubes demonstrated amazing stability in presence of oil but showed poor stability in absence of oil. Irregular shaped Al_2O_3 nanoparticles produced the best foam in absence of oil but showed poor stability in presence of oil. Foam stabilized by perfectly spherical shape SiO_2 nanoparticles demonstrated consistent stability in presence and absence of oil at high temperature. The study suggests that nanoparticles shape and orientation at gas–liquid and liquid–liquid interface are crucial parameters for foam stabilization in absence and presence of oil and should be considered during screening of nanoparticles for foam stability experiments.
2. Positive values of entering coefficient (E), negative values of spreading coefficients (S), and smaller lamellae number (L) were obtained for nanoparticles-surfactant stabilized foams. The study indicates that the presence of nanoparticles did not necessarily prevented the invasion of interface between the liquid and the gas by the oil, but nanoparticles adsorption and aggregation at the gas–liquid interface prevented the spreading of invaded oil by keeping the pseudo-emulsion films stable.
3. Increasing nanoparticles concertation increased the bulk stability of sub-critical CO_2 foam while 0.5 wt% SiO_2 was obtained as the ideal concentration for the utmost stability of the supercritical CO_2 foam at static and dynamic conditions, suggesting that stable CO_2 foam can be produced in porous media at high pressure with smaller nanoparticles concentration.
4. 2 wt% NaCl in nanoparticles-surfactant solutions resulted in generation of most stable sub-critical and super-critical bulk CO_2 foam at bulk condition while supercritical CO_2 foam further

demonstrated highest pressure drop and lowest mobility reduction in presence of 10 wt% NaCl. This implies that the stability of nanoparticles-surfactant stabilized CO_2 foam can be enhanced with the presence of salt in nanoparticle-surfactant formulation at optimum concentration.

5. Mechanisms of nanoparticles-surfactant stabilized CO_2 foam stability at subcritical and supercritical conditions are the adsorption and aggregation of nanoparticles-surfactant complex at foam lamellae oil was easily dispersed at thin liquid films of conventional foams to destroy the foam lamellae but migrated to the Plateau borders of nanoparticles-surfactant CO_2 foam to boost the foam stability.

CRediT authorship contribution statement

Nurudeen Yekeen: Project administration, Visualization, Methodology, Conceptualization, Writing - review & editing, Validation. **Tan Xin Kun:** Methodology, Conceptualization, Writing - review & editing. **Ahmed Al-Yaseri:** Project administration, Conceptualization, Writing - review & editing. **Farad Sagala:** Methodology, Validation, Writing - review & editing. **Ahmad Kamal Idris:** Supervision, Conceptualization, Methodology, Project administration.

Declaration of Competing Interest

The authors declare that they have no known competing financial interests or personal relationships that could have appeared to influence the work reported in this paper.

Acknowledgment

The efforts of UCSI University Malaysia in providing the needed support for the success of this research through Research Excellence and Innovation Grant (REIG) with project code of REIG-FETBE-/2021/030 is acknowledge.

Appendix A. Supplementary material

Supplementary data to this article can be found online at https://doi.org/10.1016/j.molliq.2021.116658.

References

[1] Q. Sun, Z. Li, J. Wang, S. Li, L. Jiang, C. Zhang, Properties of multi-phase foam and its flow behavior in porous media, RSC Adv. 5 (2015) 67676–67689, https://doi.org/10.1039/C5RA09686C.
[2] N. Yekeen, M.A. Manan, A.K. Idris, E. Padmanabhan, R. Junin, A.M. Samin, A.O. Gbadamosi, I. Oguamah, A comprehensive review of experimental studies of nanoparticles-stabilized foam for enhanced oil recovery, J. Pet. Sci. Eng. 164 (2018) 43–74, https://doi.org/10.1016/j.petrol.2018.01.035.
[3] R. Singh, K.K. Mohanty, Foam flow in a layered, heterogeneous porous medium: A visualization study, Fuel. 197 (2017) 58–69, https://doi.org/10.1016/j.fuel.2017.02.019.
[4] R. Singh, K.K. Mohanty, Study of nanoparticle-stabilized foams in harsh reservoir conditions, Transp. Porous Med. 131 (2020) 135–155, https://doi.org/10.1007/s11242-018-1215-y.
[5] A. Rezaei, Z. Derikvand, R. Parsaei, M. Imanivarnosfaderani, Surfactant-silica nanoparticle stabilized N2-foam flooding: A mechanistic study on the effect of surfactant type and temperature, J. Mol. Liq. 325 (2021), https://doi.org/10.1016/j.molliq.2020.115091 115091.
[6] J. Zhao, F. Torabi, J. Yang, The synergistic role of silica nanoparticle and anionic surfactant on the static and dynamic CO2 foam stability for enhanced heavy oil recovery: An experimental study, Fuel 287 (2021), https://doi.org/10.1016/j.fuel.2020.119443 119443.
[7] A.S. Hanamertani, R.M. Pilus, N.A. Manan, S. Ahmed, M. Awang, Ionic liquid application in surfactant foam stabilization for gas mobility control, Energy Fuels. 32 (2018) 6545–6556, https://doi.org/10.1021/acs.energyfuels.8b00584.
[8] A.S. Hanamertani, S. Ahmed, Probing the Role of Associative Polymer on scCO2-Foam Strength and Rheology Enhancement in Bulk and Porous Media for Improving Oil Displacement Efficiency, Energy 228 (2021), https://doi.org/10.1016/j.energy.2021.120531 120531.
[9] G.M. Phong, R.M. Pilus, A. Mustaffa, L. Thangavel, N.M. Mohamed, Relationship between fly ash nanoparticle-stabilized-foam and oil production in core displacement and simulation studies, Fuel 266 (2020), https://doi.org/10.1016/j.fuel.2020.117033 117033.
[10] A.R. Risal, M.A. Manan, N. Yekeen, N.B. Azli, A.M. Samin, X.K. Tan, Experimental investigation of enhancement of carbon dioxide foam stability, pore plugging, and oil recovery in the presence of silica nanoparticles, Pet Sci. 16 (2019) 344–356, https://doi.org/10.1007/s12182-018-0280-8.
[11] N. Yekeen, A.A. Malik, A.K. Idris, N.I. Reepei, K. Ganie, Foaming properties, wettability alteration and interfacial tension reduction by saponin extracted from soapnut (Sapindus Mukorossi) at room and reservoir conditions, J. Pet. Sci. Eng. 195 (2020), https://doi.org/10.1016/j.petrol.2020.107591 107591.
[12] A.H. Syed, A.K. Idris, D.F. Mohshim, N. Yekeen, M.A. Buriro, Influence of lauryl betaine on aqueous solution stability, foamability and foam stability, J. Petrol Explor. Prod. Technol. 9 (2019) 2659–2665, https://doi.org/10.1007/s13202-019-0652-7.
[13] N. Yekeen, E. Padmanabhan, A.K. Idris, Synergistic effects of nanoparticles and surfactants on n-decane-water interfacial tension and bulk foam stability at high temperature, J. Pet. Sci. Eng. 179 (2019) 814–830, https://doi.org/10.1016/j.petrol.2019.04.109.
[14] N. Yekeen, A.K. Idris, M.A. Manan, A.M. Samin, Experimental study of the influence of silica nanoparticles on the bulk stability of SDS-foam in the presence of oil, J. Dispers. Sci. Technol. 38 (2017) 416–424, https://doi.org/10.1080/01932691.2016.1172969.
[15] N. Yekeen, A.K. Idris, M.A. Manan, A.M. Samin, A.R. Risal, T.X. Kun, Bulk and bubble-scale experimental studies of influence of nanoparticles on foam stability, Chin. J. Chem. Eng. 25 (2017) 347–357, https://doi.org/10.1016/j.cjche.2016.08.012.
[16] N. Yekeen, E. Padmanabhan, A.K. Idris, S.M. Ibad, Surfactant adsorption behaviors onto shale from Malaysian formations: Influence of silicon dioxide nanoparticles, surfactant type, temperature, salinity and shale lithology, J. Pet. Sci. Eng. 179 (2019) 841–854, https://doi.org/10.1016/j.petrol.2019.04.096.
[17] N. Yekeen, M.A. Manan, A.K. Idris, A.M. Samin, Influence of surfactant and electrolyte concentrations on surfactant Adsorption and foaming characteristics, J. Pet. Sci. Eng. 149 (2017) 612–622, https://doi.org/10.1016/j.petrol.2016.11.018.
[18] G. Shi, K. Tang, F. Wang, Q. Luo, L. Bai, P. Sun, D. Zhu, Visualized Study of a Nanoparticle-Assisted Foam System to Enhance Oil Recovery by Nuclear Magnetic Resonance Online Flooding Experiment, Energy Fuels 35 (2020) 465–472, https://doi.org/10.1021/acs.energyfuels.0c03521.
[19] K. Yang, S. Li, K. Zhang, Y. Wang, Synergy of hydrophilic nanoparticle and nonionic surfactant on stabilization of carbon dioxide-in-brine foams at elevated temperatures and extreme salinities, Fuel. 288 (2021), https://doi.org/10.1016/j.fuel.2020.119624 119624.
[20] A.E. Bayat, K. Rajaei, R. Junin, Assessing the effects of nanoparticle type and concentration on the stability of CO2 foams and the performance in enhanced oil recovery, Colloids Surf, A Physicochem. Eng. Asp. 511 (2016) 222–231, https://doi.org/10.1016/j.colsurfa.2016.09.083.
[21] A.S. Emrani, H.A. Nasr-El-Din, An experimental study of nanoparticle-polymer-stabilized CO2 foam, Colloids Surf, A Physicochem. Eng. Asp. 524 (2017) 17–27, https://doi.org/10.1016/j.colsurfa.2017.04.023.
[22] A. Srivastava, W. Qiao, Y. Wu, X. Li, L. Bao, C. Liu, Effects of silica nanoparticles and polymers on foam stability with sodium dodecylbenzene sulfonate in water–liquid paraffin oil emulsions at high temperatures, J. Mol. Liq. 241 (2017) 1069–1078, https://doi.org/10.1016/j.molliq.2017.06.096.
[23] N. Pal, A. Verma, K. Ojha, A. Mandal, Nanoparticle-modified gemini surfactant foams as efficient displacing fluids for enhanced oil recovery, J. Mol. Liq. 310 (2020), https://doi.org/10.1016/j.molliq.2020.113193 113193.
[24] W. Kang, H. Jiang, H. Yang, Z. Li, B. Zhou, Y. He, B. Sarsenbekuly, M. Gabdullin, Study of nano-SiO2 reinforced CO2 foam for anti-gas channeling with a high temperature and high salinity reservoir, J. Ind. Eng. Chem. 97 (2021) 506–514, https://doi.org/10.1016/j.jiec.2021.03.007.
[25] S. Ahmed, W. Alameri, W.W. Ahmed, S. Khan, Rheological behavior of scCO2-Foam for improved hydrocarbon recovery: Experimental and deep learning approach, J. Pet. Sci. Eng 203 (2021), https://doi.org/10.1016/j.petrol.2021.108646 108646.
[26] X. Yin, W. Kang, S. Song, Z. Huang, X. Hou, H. Yang, Stabilization mechanism of CO2 foam reinforced by regenerated cellulose, Colloids Surf., A Physicochem. Eng. Asp. 555 (2018) 754–764, https://doi.org/10.1016/j.colsurfa.2018.07.042.
[27] S. Rouimi, C. Schorsch, C. Valentini, S. Vaslin, Foam stability and interfacial properties of milk protein–surfactant systems, Food Hydrocoll. 19 (2005) 467–478, https://doi.org/10.1016/j.foodhyd.2004.10.032.
[28] H. Jin, W. Zhou, J. Cao, S.D. Stoyanov, T.B. Blijdenstein, P.W. de Groot, L.N. Arnaudov, E.G. Pelan, Super stable foams stabilized by colloidal ethyl cellulose particles, Soft Matter 8 (2012) 2194–2205, https://doi.org/10.1039/C1SM06518A.
[29] T. Blijdenstein, P. De Groot, S. Stoyanov, On the link between foam coarsening and surface rheology: why hydrophobins are so different, Soft Matter 6 (2010) 1799–1808, https://doi.org/10.1039/B925648B.
[30] I.-H. Yoon, S.B. Yoon, Y. Sihn, M.-S. Choi, C.-H. Jung, W.-K. Choi, Stabilizing decontamination foam using surface-modified silica nanoparticles containing chemical reagent: foam stability, structures, and dispersion properties, RSC Adv. 11 (2021) 1841–1849, https://doi.org/10.1039/D0RA07644A.
[31] C. Delgado-Sánchez, A.A. Cuadri, F.J. Navarro, P. Partal, Formulation and processing of novel non-aqueous polyethylene glycol-in-silicone oil (o/o)

phase change emulsions, Sol. Energy Mater. Sol. Cells. 221 (2021), https://doi.org/10.1016/j.solmat.2020.110898 110898.
[32] C. Delgado-Sánchez, V. Fierro, S. Li, A. Pasc, A. Pizzi, A. Celzard, Stability analysis of tannin-based foams using multiple light-scattering measurements, Eur. Polym. J. 87 (2017) 318–330, https://doi.org/10.1016/j.eurpolymj.2016.12.036.
[33] J. Zhao, F. Torabi, J. Yang, The synergistic role of silica nanoparticle and anionic surfactant on the static and dynamic CO2 foam stability for enhanced heavy oil recovery: An experimental study, Fuel 287 (2020), https://doi.org/10.1016/j.fuel.2020.119443 119443.
[34] C. Celia, E. Trapasso, D. Cosco, D. Paolino, M. Fresta, Turbiscan Lab® Expert analysis of the stability of ethosomes® and ultradeformable liposomes containing a bilayer fluidizing agent, Colloid Surface B. 72 (2009) 155–160, https://doi.org/10.1016/j.colsurfb.2009.03.007.
[35] J. Liu, X.-F. Huang, L.-J. Lu, M.-X. Li, J.-C. Xu, H.-P. Deng, Turbiscan Lab® Expert analysis of the biological demulsification of a water-in-oil emulsion by two biodemulsifiers, J. Hazard. Mater. 190 (2011) 214–221, https://doi.org/10.1016/j.jhazmat.2011.03.028.
[36] X. Qi, Y.N. Dong, H. Wang, C. Wang, F. Li, Application of Turbiscan in the homoaggregation and heteroaggregation of copper nanoparticles, Colloids Surf., A Physicochem. Eng. Asp. 535 (2017) 96–104, https://doi.org/10.1016/j.colsurfa.2017.09.015.
[37] Y. Ren, J. Zheng, Z. Xu, Y. Zhang, J. Zheng, Application of Turbiscan LAB to study the influence of lignite on the static stability of PCLWS, Fuel. 214 (2018) 446–456, https://doi.org/10.1016/j.fuel.2017.08.026.
[38] M. Luo, X. Qi, T. Ren, Y. Huang, A.A. Keller, H. Wang, B. Wu, H. Jin, F. Li, Heteroaggregation of CeO2 and TiO2 engineered nanoparticles in the aqueous phase: Application of turbiscan stability index and fluorescence excitation-emission matrix (EEM) spectra, Colloids Surf., A Physicochem. Eng Asp. 533 (2017) 9–19, https://doi.org/10.1016/j.colsurfa.2017.08.014.
[39] Y. Lu, W. Kang, J. Jiang, J. Chen, D. Xu, P. Zhang, L. Zhang, H. Feng, H. Wu, Study on the stabilization mechanism of crude oil emulsion with an amphiphilic polymer using the β-cyclodextrin inclusion method, RSC Adv. 7 (2017) 8156–8166, https://doi.org/10.1039/C6RA28528G.
[40] Y. Lu, H. Wu, Z. Meng, J. Jiang, Y. Jin, Z. Deng, W. Su, Z. Li, W. Kang, Salt effect on hydrophobically modified polyacrylamide-containing crude oil emulsions: stability and rheology study, Colloid Polym. Sci. 296 (2018) 515–527, https://doi.org/10.1007/s00396-018-4267-1.
[41] X. Zhang, W. Zheng, T. Zhang, J. Ge, P. Jiang, G. Zhang, CO2 in water foam stabilized with CO2-dissolved surfactant at high pressure and high temperature, J. Pet. Sci. Eng. 178 (2019) 930–936, https://doi.org/10.1016/j.petrol.2019.03.066.
[42] R. Rastogi, R. Kaushal, S. Tripathi, A.L. Sharma, I. Kaur, L.M. Bharadwaj, Comparative study of carbon nanotube dispersion using surfactants, J. Colloid Interface Sci. 328 (2008) 421–428, https://doi.org/10.1016/j.jcis.2008.09.015.
[43] X. Wang, K. Mohanty, Improved Oil Recovery in Fractured Reservoirs by Strong Foams Stabilized by Nanoparticles, Energy Fuels. 35 (2021) 3857–3866, https://doi.org/10.1021/acs.energyfuels.0c03961.
[44] N. Briggs, A.K.Y. Raman, L. Barrett, C. Brown, B. Li, D. Leavitt, C.P. Aichele, S. Crossley, Stable pickering emulsions using multi-walled carbon nanotubes of varying wettability, Colloids Surf., A Physicochem. Eng. Asp. 537 (2018) 227–235, https://doi.org/10.1016/j.colsurfa.2017.10.010.
[45] M. Bystrzejewski, A. Huczko, H. Lange, T. Gemming, B. Büchner, M. Rümmeli, Dispersion and diameter separation of multi-wall carbon nanotubes in aqueous solutions, J. Colloid Interface Sci. 345 (2010) 138–142, https://doi.org/10.1016/j.jcis.2010.01.081.
[46] T. Sharma, G.S. Kumar, B.H. Chon, J.S. Sangwai, Thermal stability of oil-in-water Pickering emulsion in the presence of nanoparticle, surfactant, and polymer, J Ind Eng Chem. 22 (2015) 324–334, https://doi.org/10.1016/j.jiec.2014.07.026.
[47] J.P. Gallo-Molina, N. Ratkovich, O. Alvarez, The Application of Computational Fluid Dynamics to the Multiscale Study of Oil-in-Water Emulsions, J. Ind. Eng. Chem. 57 (2018) 578–589, https://doi.org/10.1021/acs.iecr.7b03846.
[48] R. Rafati, O.K. Oludara, A.S. Haddad, H. Hamidi, Experimental investigation of emulsified oil dispersion on bulk foam stability, Colloids Surf., A Physicochem. Eng. Asp. 554 (2018) 110–121, https://doi.org/10.1016/j.colsurfa.2018.06.043.
[49] X. Duan, J. Hou, T. Cheng, S. Li, Y. Ma, Evaluation of oil-tolerant foam for enhanced oil recovery: laboratory study of a system of oil-tolerant foaming agents, J. Pet. Sci. Eng. 122 (2014) 428–438, https://doi.org/10.1016/j.petrol.2014.07.042.
[50] R. Farajzadeh, A. Andrianov, R. Krastev, G. Hirasaki, W.R. Rossen, Foam–oil interaction in porous media: implications for foam assisted enhanced oil recovery, Adv. Colloid Interface Sci. 183 (2021) 1–13, https://doi.org/10.1016/j.cis.2012.07.002.
[51] Y. Wang, Y. Zhang, Y. Liu, L. Zhang, S. Ren, J. Lu, X. Wang, N. Fan, The stability study of CO2 foams at high pressure and high temperature, J. Pet. Sci. Eng. 154 (2017) 234–243, https://doi.org/10.1016/j.petrol.2017.04.029.
[52] J. Yu, M. Khalil, N. Liu, R. Lee, Effect of particle hydrophobicity on CO2 foam generation and foam flow behavior in porous media, Fuel 126 (2014) 104–108, https://doi.org/10.1016/j.fuel.2014.02.053.
[53] N. Yekeen, M.A. Manan, A.K. Idris, A.M. Samin, A.R. Risal, Experimental investigation of minimization in surfactant adsorption and improvement in surfactant-foam stability in presence of silicon dioxide and aluminum oxide nanoparticles, J. Pet. Sci. Eng. 159 (2017) 115–134, https://doi.org/10.1016/j.petrol.2017.09.021.
[54] K. Yang, S. Li, K. Zhang, Y. Wang, Synergy of hydrophilic nanoparticle and nonionic surfactant on stabilization of carbon dioxide-in-brine foams at elevated temperatures and extreme salinities, Fuel 228 (2020), https://doi.org/10.1016/j.fuel.2020.119624 119624.
[55] C. Da, S. Alzobaidi, G. Jian, L. Zhang, S.L. Biswal, G.J. Hirasaki, K.P. Johnston, Carbon dioxide/water foams stabilized with a zwitterionic surfactant at temperatures up to 150 C in high salinity brine, J. Pet. Sci. Eng. 166 (2018) 880–890, https://doi.org/10.1016/j.petrol.2018.03.071.
[56] S. Alzobaidi, M. Lotfollahi, I. Kim, K.P. Johnston, D.A. DiCarlo, Carbon dioxide-in-brine foams at high temperatures and extreme salinities stabilized with silica nanoparticles, Energy Fuels 31 (2017) 10680–10690, https://doi.org/10.1021/acs.energyfuels.7b01814.
[57] C. Xiao, S.N. Balasubramanian, L.W. Clapp, Rheology of Viscous CO2 Foams Stabilized by Nanoparticles under High Pressure, Ind. Eng. Chem. Res. 56 (2017) 8340–8348, https://doi.org/10.1021/acs.iecr.7b01404.
[58] C. Da, S. Alzobaidi, G. Jian, L. Zhang, S.L. Biswal, G.J. Hirasaki, K.P. Johnston, Carbon dioxide/water foams stabilized with a zwitterionic surfactant at temperatures up to 150° C in high salinity brine, J. Pet. Sci. Eng. 166 (2018) 880–890, https://doi.org/10.1016/j.petrol.2018.03.071.
[59] J. San, S. Wang, J. Yu, N. Liu, R. Lee, Nanoparticle-stabilized carbon dioxide foam used in enhanced oil recovery: effect of different ions and temperatures, SPE J. 22 (2017) 1416–1423, https://doi.org/10.2118/179628-PA.
[60] A.F. Ibrahim, H.A. Nasr-El-Din, Stability Improvement of Carbon Dioxide Foam Using Nanoparticles and Viscoelastic Surfactants for Enhanced-Oil-Recovery Applications, SPE Res. Eval. Eng. 23 (2020) 414–430, https://doi.org/10.2118/191251-PA.
[61] S.A. Farzaneh, M. Sohrabi, Experimental investigation of CO_2-foam stability improvement by alkaline in the presence of crude oil, Chem. Eng. Res. Des. 94 (2015) 375–389, https://doi.org/10.1016/j.cherd.2014.08.011.
[62] M. Simjoo, T. Rezaei, A. Andrianov, P. Zitha, Foam stability in the presence of oil: effect of surfactant concentration and oil type, Colloids Surf., A Physicochem. Eng. Asp. 438 (2013) 148–158, https://doi.org/10.1016/j.colsurfa.2013.05.062.
[63] E. Tyrode, M.W. Rutland, C.D. Bain, Adsorption of CTAB on hydrophilic silica studied by linear and nonlinear optical spectroscopy, J. Am. Chem. Soc. 130 (2008) 17434–17445, https://doi.org/10.1021/ja805169z.
[64] N. Yekeen, E. Padmanabhan, A.H. Syed, T. Sevoo, K. Kanesen, Synergistic influence of nanoparticles and surfactants on interfacial tension reduction, wettability alteration and stabilization of oil-in-water emulsion, J. Pet. Sci. Eng. 186 (2020), https://doi.org/10.1016/j.petrol.2019.106779 106779.
[65] H. Jiang, Y. Sheng, T. Ngai, Pickering emulsions: Versatility of colloidal particles and recent applications, Curr. Opin. Colloid In. 49 (2020) 1–15, https://doi.org/10.1016/j.cocis.2020.04.010.